electronics

MDPI

Article

Improving Patch Antenna Performance Through Resonators: Insights into and Benefits of Dielectric and Conductive Materials and Geometric Shapes

Cláudia M. S. Fonseca [1,*], Chryslène M. M. Adetonah [1], Luís Guilherme S. Costa [1], Benigno R. Díaz [2], Marco Aurélio O. Schroeder [3], Glaucio L. Ramos [4] and Moisés V. Ribeiro [1,*]

[1] Department of Electrical Engineering, Federal University of Juiz de Fora, Juiz de Fora 36036-900, Brazil; chryslene.adetonah@estudante.ufjf.br (C.M.M.A.); luis.costa@estudante.ufjf.br (L.G.S.C.)
[2] Department of Telecommunications, Institute of Electrical Engineering, University of the Republic, Montevideo 11300, Uruguay; benigno@fing.edu.uy
[3] Department of Electrical Engineering, Federal University of São João del Rei, São João del Rei 36307-352, Brazil; schroeder@ufsj.edu.br
[4] Department of Telecommunications and Mechatronics Engineering, Federal University of São João del Rei, Ouro Branco 36415-000, Brazil; glaucio@ufsj.edu.br
* Correspondence: claudia.fonseca@estudante.ufjf.br (C.M.S.F.); moises.ribeiro@ufjf.br (M.V.R.)

Abstract: This paper investigates the usefulness of combining dielectric and conductive materials with various geometries to build resonators and enhance patch antenna performance when considering the decoupled design approach. Three materials (distilled water, glycerin, and graphite) and fifteen geometries are considered. The obtained results through numerical simulations show how the selected materials and geometries can be combined to strategically design resonators that can effectively confine electromagnetic fields, shift the resonant frequency, improve antenna directionality and effective gain, facilitate multi-band operation, broaden the bandwidth, and improve impedance matching and the radiation pattern. Overall, the analyses and discussions offer insights and guidelines for combining dielectric and conductive materials with several geometries to build a resonator that can improve patch antenna performance when a low-quality substrate is considered.

Keywords: patch antenna; resonator; distilled water; glycerin; graphite; geometric shapes

check for updates

Academic Editor: Reza K. Amineh

Received: 30 January 2025
Revised: 26 March 2025
Accepted: 5 April 2025
Published: 9 April 2025

Citation: Fonseca, C.M.S.; Adetonah, C.M.M.; Costa, L.G.S.; Díaz, B.R.; Schroeder, M.A.O.; Ramos, G.L.; Ribeiro, M.V. Improving Patch Antenna Performance Through Resonators: Insights into and Benefits of Dielectric and Conductive Materials and Geometric Shapes. *Electronics* **2025**, *14*, 1521. https://doi.org/10.3390/electronics14081521

Copyright: © 2025 by the authors. Licensee MDPI, Basel, Switzerland. This article is an open access article distributed under the terms and conditions of the Creative Commons Attribution (CC BY) license (https://creativecommons.org/licenses/by/4.0/).

1. Introduction

Patch antennas are fundamental components in various compact devices for wireless communication. As they work by transmitting and receiving electromagnetic waves, patch antennas directly influence system performance [1–3]. Recently, their applications have expanded significantly to meet the growing needs of emerging technologies, including energy harvesting and smart cities [3,4]. Traditionally, patch antennas are constructed using copper and rigid dielectric materials; however, as demand for flexible and adaptable systems increases, novel antennas have emerged that diverge from conventional ones. These new antennas employ flexible and reconfiguration materials, which are not present in traditional copper-based designs. Among the unconventional materials investigated for new antennas are textiles, polymers, graphene, and liquid materials. Currently, liquid dielectrics, including water and other materials, have become a focal point of recent investigations due to their unique properties and potential for improving antenna design and performance [3].

In this regard, integrating unconventional materials in patch antennas aligns with the growing interest in resonators, as both approaches aim to enhance antenna performance across several frequency bands while meeting the demands of modern applications. Strategically placed resonators effectively confine electromagnetic fields, improving patch antenna performance. Furthermore, this arrangement of embedded patch antennas in resonators can operate across multiple frequency bands, making them ideal for modern applications that demand high versatility, such as wireless communications, sensor networks, and satellite communication systems. The ability to manipulate the properties of the resonator offers new opportunities for the development of efficient multi-band antennas [5,6].

Recent research has explored using various liquid and solid materials as resonators in patch antenna designs. For instance, Paracha et al. [7] review the design and applications of liquid metal antennas, highlighting their adaptability and versatility for modern wireless communications. Their study explored innovative fabrication techniques and the advantages of conductive fluids for creating mechanically flexible, reconfigurable antennas. Similarly, Wang et al. [8] introduced a hybrid dual-tube water antenna, where distilled water acts as the dielectric load while salty water serves as the radiating element. This configuration significantly increased the radiation efficiency, reaching up to 84% across its operating band. Another example is the work of Li and Luk [9], which investigated the use of water as a dense dielectric patch antenna. The water patch functioned similarly to a traditional metallic patch in its design, achieving a broader bandwidth (BW) and improved radiation efficiency. Aldrigo et al. [6] presented a tunable 24 GHz antenna array based on noncrystalline graphite, demonstrating the significant potential for high-performance microwave components and their usefulness for advancing the next generations of wireless communication technologies. Moreover, Mukherjee et al. [10] review advanced techniques and geometries in dielectric resonator antennas, focusing on size miniaturization, BW optimization, and radiation pattern stability. In addition, the authors of [11] explored the development of multi-beam conformal antennas using liquid metal, showing that antennas using liquid metal can sustain their performance when the geometry is reshaped. Furthermore, Malfajani et al. [12] proposed an encapsulated dielectric resonator antenna design, which enables efficient radiation across two widely separated frequency bands. Meanwhile, Halimi et al. [13] provided an overview of dielectric resonators for applications in radio frequency (RF) energy harvesting and systems and wireless power transmission. Additionally, the authors of [14] proposed a broadband antenna designed as an array element for advanced microwave brain imaging systems. It is immersed in a medium with a carefully selected relative permittivity, improving impedance matching between the antenna and brain tissues to enhance signal transmission and reception. Varshney [15] conducted a numerical analysis of a broadband waveform in a THz absorber, utilizing a dielectric cavity resonator integrated with a graphite disk. Moreover, Su [16] proposed a method to enhance the gain of a dielectric resonator antenna by utilizing metallic patches. The works above and references therein highlight that resonators can also enhance antenna performance through innovative material usage, driving advancements in diverse applications such as wireless communications, energy harvesting, and imaging systems.

Despite these advancements, several challenges remain in improving the efficiency of embedded patch antennas in resonators. One notable issue is developing a clear view of how types of materials and geometries of resonators affect the electromagnetic performance of patch antennas with high dielectric constants. It is well-established that designing patch antennas with high dielectric materials is difficult, as a high dielectric constant often degrades overall efficiency, especially in terms of radiation pattern characteristics, such as main lobe magnitude (MLM), main lobe direction (MLD), half-Power Beamwidth (HPBW),

and side lobe level (SLL) [17]. However, understanding the benefits of resonators in this context needs a comprehensive investigation. While several studies focus on simplified configurations of resonators [5], there is a gap in the literature in terms of a comprehensive analysis in which a unique set of specification designs and constraint are applied. Such an investigation is relevant as it would allow researchers to easily highlight and compare the benefits of geometric shapes and materials used to build resonators that will be employed to improve the performance of patch antennas.

This paper addresses this gap by investigating the combining of dielectric and conductive materials with distinct geometries to build resonators and, consequently, to improve patch antenna performance when the decoupled method is adopted. The decoupled method means that the patch antenna and resonator are sequentially designed in that order. Consequently, it offers insights and guidelines for fostering patch antennas embedded in resonators. In this regard, this paper introduces the following contributions:

- A comprehensive presentation of the combinations of dielectric and conductive materials (i.e., distilled water, glycerin, and graphite) and fifteen geometries for building resonators and improving a few characteristics or overall performance of patch antennas.
- Numerical simulations of the possible combination of the selected sets of materials and geometries and analyses based on the radiation pattern and the magnitude of the scattering parameter S_{11} (i.e., $|S_{11}|$) when the decoupled approach is used, in which the resonator is designed to fulfill the specifications of an already designed patch antenna.

Considering that the benefits of resonators are more relevant when the material of the substrate of the rectangular patch antenna is of low quality, the following findings are related to the use of flame retardant-4 (FR-4) when extensive numerical simulations are considered:

- For distilled water (DW) resonators, the impact on scattering parameter S_{11} and radiation pattern varies depending on the geometry of the resonator. Specific geometries offer a broader BW, improved impedance matching, and support for multiple resonant frequencies. Others enhance characteristics of the radiation patterns, with some configurations achieving exceptional gain and radiation directionality while supporting multi-band operation. Moreover, specific geometries downshift the resonant frequencies, which can be used to reduce the antenna size.
- The integration of glycerin-made resonators into patch antennas yields distinct effects on the scattering parameter S_{11} and radiation patterns, depending on the geometry shape. Some geometries show potential for reducing the size of patch antennas because they downshift the resonant frequency, while others enhance radiation efficiency or improve the scattering parameter S_{11}. Other geometries provide a balance between enhanced scattering parameter S_{11} and radiation patterns. These variations in the results demonstrate the versatility of glycerin resonators in improving patch antenna performance, particularly for size reduction and improved efficiency.
- The combination of graphite-made resonators with patch antennas results in significant changes in scattering parameters S_{11} and the radiation pattern. These resonators typically cause shifts in resonant frequency, with certain configurations exhibiting more pronounced shifts. The radiation pattern is also improved, with specific geometries offering high effective gain and enhanced directionality compared to a patch antenna without a resonator. Overall, graphite resonators present substantial potential for improving patch antenna performance concerning BW, radiation efficiency, and radiation directionality, making patch antennas more compact and efficient for a broader range of applications.

The remainder of the paper is organized as follows. Section 2 formulates the investigated problem. Section 3 describes the materials and geometries used in the resonators. Section 4 analyzes the numerical results. Lastly, Section 5 presents the concluding remarks.

2. Problem Formulation

Patch antennas are essential in wireless and satellite communication systems, particularly in microwave and millimeter-wave RF-based front-end architectures. Patch antenna design continuously refines these systems to enhance energy efficiency, coverage, flexibility, and reliability, driving advancements in front-end engineering. Achieving these improvements requires meticulous selection of substrates and embedding materials, as both directly influence key antenna performance parameters such as impedance matching, radiation efficiency, and BW.

Embedding materials, classified as dielectric or conductive, serve multiple critical functions in antenna design. High-permittivity materials contribute to miniaturization by reducing the antenna's physical footprint without compromising performance. Proper material selection enhances gain and directivity by mitigating surface wave losses and optimizing radiation characteristics. Additionally, embedding materials support impedance matching, minimizing reflection losses and improving signal transmission efficiency. In harsh environments, encapsulating materials protect antennas from moisture, temperature variations, and mechanical stress, ensuring long-term reliability.

The literature has pointed out that the behavior of a patch antenna is strongly influenced by the electrical and mechanical characteristics of the used substrate, which directly impact key evaluation parameters obtained from the radiation pattern and S_{11} scattering parameter (e.g., BW, directionality, and resonant frequency). For example, Figure 1 illustrates the radiation patterns of a single rectangular patch antenna with substrates of different dielectric constants and loss tangents. The difference between radiation patterns is attributed to the fact that dielectric constant and loss tangent are inversely proportional to the radiation efficiency of the patch antenna, which is expressed as [17]

$$\eta_{\text{rad}}^{\text{patch}} = \frac{1}{1 + \frac{\tan\delta + \tan\delta_\mu}{240 G_{\text{r}}^{\text{patch}}} \frac{W}{h} \sqrt{\frac{\varepsilon_{\text{r}}}{\mu_{\text{r}}}}}, \tag{1}$$

where ε_{r} is the dielectric constant, μ_{r} is the magnetic constant, $\tan\delta$ is the dielectric loss tangent, $\tan\delta_\mu$ is the magnetic loss tangent, $G_{\text{r}}^{\text{patch}}$ is the radiation conductance, W is the width of the radiation element, and h is the height of the substrate.

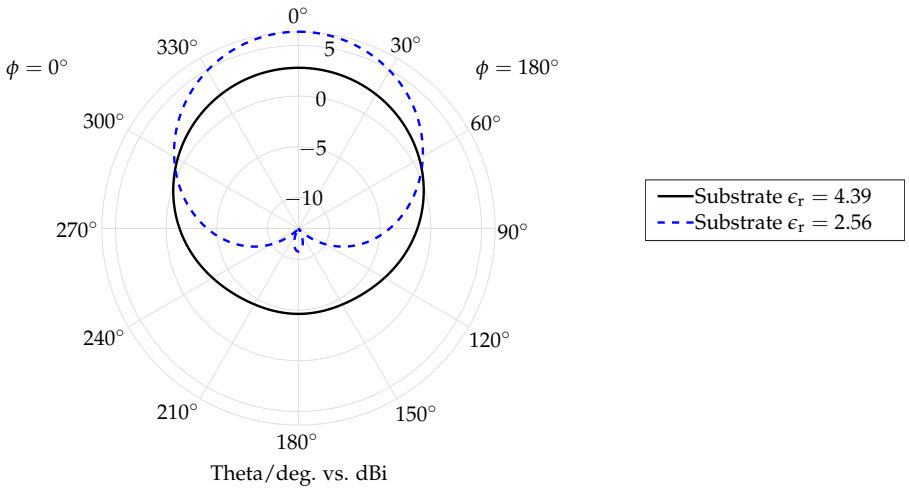


Figure 1. Radiation pattern plot of the far-field realized gain at 2.45 GHz, cut in ($\phi = 0$).

Moreover, fringing fields can significantly impair the performance of patch antennas if appropriate countermeasures are not implemented. These fields increase the effective dimensions of the patch, thereby altering its impedance characteristics and leading to energy dissipation within the substrate instead of efficient radiation into the surrounding environment [4,17]. This issue becomes more pronounced in substrates with a high loss tangent, where a more significant portion of the electromagnetic energy dissipates as heat rather than being radiated as an electromagnetic field. As a result, the radiation efficiency and overall performance of the antenna experience substantial reductions [4,17]. Furthermore, this problem intensifies when the substrate quality is poor (e.g., FR-4 material).

Given the limitations regarding substrates with high ε_r and tangent loss ($\tan\delta$), the challenge of designing antennas with suitable performance highlights the need to explore alternative approaches, including the integration of resonators. Indeed, embedding patch antennas in dielectric and conductive resonators is promising, mainly when poor substrates (i.e., those with high dielectric constants) are used [17]. The resonator works as an impedance-matching component, confining electromagnetic waves within a specific geometry that defines the resonant modes. The electromagnetic field distribution inside the resonator depends on its shape, configuration, dimensions, and the particular resonant mode being excited. These modes are classified into the transverse electric (TE) and transverse magnetic (TM) types [5]. Furthermore, the materials used in the composition of the resonator exhibit electromagnetic properties that significantly affect wave propagation and, consequently, impact the overall performance of patch antennas [18–20].

For example, Rodríguez et al. [21] proposed a SPIDA antenna embedded in dielectric waveguides, achieving size reduction, multi-band operation, and radiation pattern modification to enable beamforming through frequency tuning. Furthermore, Dash and Sahu [22] explored the application of resonators to enhance antenna performance, demonstrating that combining tapered dielectric resonators with band notches effectively improves ultra-wideband antenna characteristics. They also showed that an inverted conical resonator significantly enhances antenna gain and impedance bandwidth. Moreover, Sun and Luk [23] proposed a compact water patch antenna that incorporates an annular water ring beneath the patch, resulting in a reduced center frequency and overall antenna size. Their results confirmed a stable radiation pattern and wide bandwidth. The authors of [24] introduced a dielectric waveguide patch antenna fed by an L-shaped metallic probe and enclosed in a transparent Plexiglass container. This design achieved a wide impedance bandwidth, high gain, excellent radiation efficiency, and a broadside radiation pattern across the entire bandwidth. Chu et al. [25] introduced a hybrid resonator utilizing distilled and saline water, achieving size reduction, wide bandwidth, and high efficiency. Song et al. [26] developed a wideband circularly polarized antenna incorporating liquid ionic resonators. Their experimental validation showed a significant increase in bandwidth while maintaining a compact design. Additionally, Liu et al. [27] introduced a single-fed, dual-band, circularly polarized reconfigurable liquid dielectric resonator antenna fabricated using 3 D printing technology. The measured results validated its dual-band reconfigurability and wide bandwidths. Furthermore, Gaya et al. [28] proposed a trapezoidal dielectric resonator antenna for millimeter-wave applications, which was designed to generate multiple frequency bands while maintaining a wide BW.

The literature has shown that introducing resonators with a specific dielectric constant and geometry around a patch antenna can bring some benefits. Typically, resonators with higher dielectric constants reduce the resonant frequency by modifying the wavelength of nearby electromagnetic waves. Furthermore, resonators can broaden or narrow the BW, depending on its influence on impedance matching and radiation efficiency. High-loss dielectrics introduce additional losses and decrease BW, while low-loss materials

enhance impedance matching and may increase BW [18–20]. Moreover, embedding a patch antenna within a resonator with a specific combination of material and geometry can significantly modify S_{11} and the radiation pattern (e.g., BW, effective gain, directionality, and resonant frequency).

Looking at all the papers discussed above and references therein on patch antennas embedded in resonators made of dielectric and conductive materials, we see that most studies focus on specific geometric shapes and materials under distinct design specifications and constraints, making it difficult to assess their benefits based on well-established performance criteria comparatively. Given the advantages that resonators offer to patch antennas, there is a clear necessity to provide a comprehensive analysis of how the combination of dielectric and conductive materials with different geometries to form a resonator influences the performance of a patch antenna. The following sections provide a detailed discussion and analysis to address this demand, offering valuable insights and guidance.

3. Resonators: Materials and Geometries

Resonators are highly appealing components for improving the performance of patch antennas due to their ability to modify the overall antenna performance. Indeed, the combination of material and geometry for building a resonator can significantly influence the radiation pattern and scattering parameter S_{11} of patch antennas. By examining various materials with distinct electromagnetic properties and geometries, it is possible to develop customized solutions that meet the specific requirements of different applications. To conduct a comprehensive investigation, it is essential to carefully select appropriate combinations of materials and geometries. Accordingly, Section 3.1 details the dielectric and conductive materials considered in this study, while Section 3.2 discusses the geometries used to shape these materials and, ultimately, construct resonators.

3.1. Material Types

Resonators typically consist of dielectric and conductive materials whose distinct electromagnetic properties can enhance the performance of antennas, particularly by leveraging their electromagnetic properties. Consequently, different materials allow for distinct modifications in the antenna radiation pattern and adjustments in BW and the scattering parameter S_{11}.

Dielectric resonators with a high dielectric constant work as efficient energy storage elements, primarily due to the fringe effect, which allows them to confine electromagnetic energy effectively within their structure. This confinement reduces energy losses and contributes to greater overall efficiency in antenna performance. In contrast, conductive resonators, with their lower dielectric constants, store less energy and instead work as waveguides, introducing electromagnetic characteristics that substantially enhance antenna performance [4,19,29]. In this study, we evaluate the specific impacts of resonators on the performance characteristics of patch antennas when distilled water, glycerin, and graphite are used as a material. These materials are interesting because they offer distinct properties that benefit a wide range of modern antenna designs.

- Distilled Water: Distilled water exhibits a high dielectric constant (≈80 at 20 °C), which significantly reduces the wavelength of electromagnetic waves within the substrate. This property enables the design of smaller patch antennas at the same resonant frequency while minimizing fringing fields at the patch edges. When pure, DW has a high loss tangent, resulting in reduced energy dissipation and improved resonator efficiency. Furthermore, DW offers tunable dielectric properties, which can be adjusted by varying its temperature or mixing it with other materials. Its liquid nature provides additional flexibility, allowing dynamic reconfiguration of resonators to meet specific

design requirements. This adaptability is particularly advantageous in applications requiring reconfigurable or adaptive antenna systems [29]. However, DW is sensitive to environmental factors such as evaporation and contamination, which can impact its stability and performance over time, and its liquid nature becomes a problem for containment. Overall, it is most suitable for tunable and adaptive patch antennas.

- Glycerin: Glycerin has a moderate dielectric constant (≈42.5 at 20 °C), which reduces the wavelength of electromagnetic waves in the substrate and facilitates the design of compact patch antennas for a given resonant frequency. Its low loss tangent minimizes energy dissipation, thereby enhancing the efficiency of resonators. The polar nature of glycerin, combined with its high viscosity, contributes to stable electromagnetic properties. Its hygroscopic behavior allows it to absorb and retain moisture, which can help maintain consistent dielectric characteristics over time. However, glycerin's dielectric constant is lower than that of DW, limiting its ability to achieve the same level of antenna miniaturization. Its high viscosity can also complicate its use in certain resonator geometries, potentially influencing electromagnetic performance. Despite these challenges, glycerin is well-suited for low-power, reconfigurable, and stable resonators, especially in environments prone to evaporation or rapid temperature changes [30]. Glycerin is more oriented toward stable and low-power resonators in controlled environments.
- Graphite: Graphite exhibits a highly anisotropic dielectric constant and loss tangent, with its properties differing significantly between its basal plane and the direction perpendicular to it. In the basal plane, the dielectric constant ranges from 1 to 5, and the loss tangent varies between 0.1 and 1.0. Perpendicular to the basal plane, the dielectric constant increases to 10–15, with a higher loss tangent of between 0.01 and 0.1. Due to its high electrical conductivity, particularly in the basal plane, graphite is an excellent material for conductive components in resonator designs. Its low density makes it lightweight and easy to process into thin sheets, powders, or composites, allowing integration into various resonator geometries. Graphite also effectively absorbs and dissipates electromagnetic radiation, enhancing its utility in electromagnetic shielding applications. However, graphite has notable limitations. Its electrical conductivity is highly anisotropic, with much higher values in the basal plane compared to the perpendicular direction. Additionally, its brittleness limits its mechanical longevity and reliability, particularly under stress or vibration. Unlike materials with high dielectric constants, graphite does not reduce the wavelength of electromagnetic waves, limiting its ability to miniaturize resonators. Furthermore, graphite is prone to oxidation at high temperatures in the presence of oxygen, which can degrade its performance. Graphite is a valuable material for resonators requiring high conductivity, thermal stability, and electromagnetic shielding. It is particularly suitable for high-power, robust resonators with critical shielding properties, although its anisotropic conductivity and mechanical limitations restrict its broader usage [31]. Graphite is most useful for high-power applications and electromagnetic shielding, where conductivity is a valuable feature.

Table 1 presents a detailed comparison of the main characteristics of DW, glycerin, and graphite, highlighting their key properties and suitability for various applications.

Table 1. Comparison between DW, glycerin, and graphite for designing RF resonators applied to improve patch antennas.

Feature	Distilled Water	Glycerin	Graphite
Dielectric Properties	High permittivity, low conductivity; suitable for capacitive loading.	High permittivity, slightly higher losses than DW.	Moderate permittivity, high conductivity.
Loss Tangent	High loss tangent, especially at microwave frequencies.	Higher loss tangent than DW.	High loss tangent; excellent for conductive applications.
Thermal Stability	Poor; properties change significantly with temperature.	Poor; viscosity and permittivity are temperature-sensitive.	Excellent thermal stability; properties remain stable at high temperatures.
Field Confinement	Limited due to higher losses; useful in liquid-based tunable designs.	Better than DW but still limited by higher losses.	Excellent for field confinement due to high conductivity.
Bandwidth	Moderate; losses limit high-frequency performance.	Moderate; broader range than DW due to better viscosity management.	Wide BW due to stable electromagnetic properties.
Fabrication Complexity	Simple; easy to integrate into liquid-based resonators.	Simple; liquid handling requires care to avoid contamination.	Complex; requires precise shaping and integration.
Weight	Lightweight, dependent on liquid containment.	Heavy liquid; more challenging to handle in portable systems.	Heavy; requires structural considerations.
Thermal Expansion	High; significant expansion with temperature changes.	High; similar issues as DW.	Low; minimal thermal expansion.

3.2. Geometric Shapes

A resonator can take on various shapes, each impacting the performance of the embedded patch antennas. Furthermore, altering the size of these geometric shapes influences key characteristics of the patch antennas, including resonant frequency, impedance matching, radiation pattern, BW, and mechanical flexibility [32]. These effects result from the interaction between geometric shapes and electromagnetic fields, as each shape supports resonant electromagnetic modes. Note that the resonant electromagnetic modes, namely TE and TM, refer to types of electromagnetic waves propagating in different geometries. TE mode is characterized by the electric field propagating in a direction transverse to the wave propagation, while the magnetic field has a longitudinal component. In contrast, TM mode is defined by the magnetic field propagating transversely to the wave direction, while the electric field has a component along the direction of wave propagation [19]. Depending on the geometry, dimensions, and arrangement of the resonators, they may operate in TE or TM mode due to boundary conditions specific to each geometry, impacting the radiation efficiency of the antenna and frequency tuning capabilities [19].

Figure 2 illustrates fifteen geometric shapes for designing resonators to improve patch antenna performance. The shapes encompass cap-based geometries, Figure 2a–d; rectangular prism-based geometries, Figure 2e,f; cone-based geometries, Figure 2g–i; half-cylinder-based geometries, Figure 2j–l; and trapezoidal prism-based geometries, Figure 2m–o. Note that the cylinder- and rectangular prism-based geometries offer two possible alignment directions: along the width of the patch antenna (WPA) or along the length of the patch antenna (LPA). Most of these geometric shapes are versatile, supporting either TE or TM modes. However, unlike other geometric shapes, the rectangular prism primarily supports the TE mode [19]. A comparison of these geometric shapes for a resonator is important

because each offers unique benefits for meeting specific design requirements and modifying relevant performance parameters (i.e., gain, BW, efficiency, and radiation pattern).

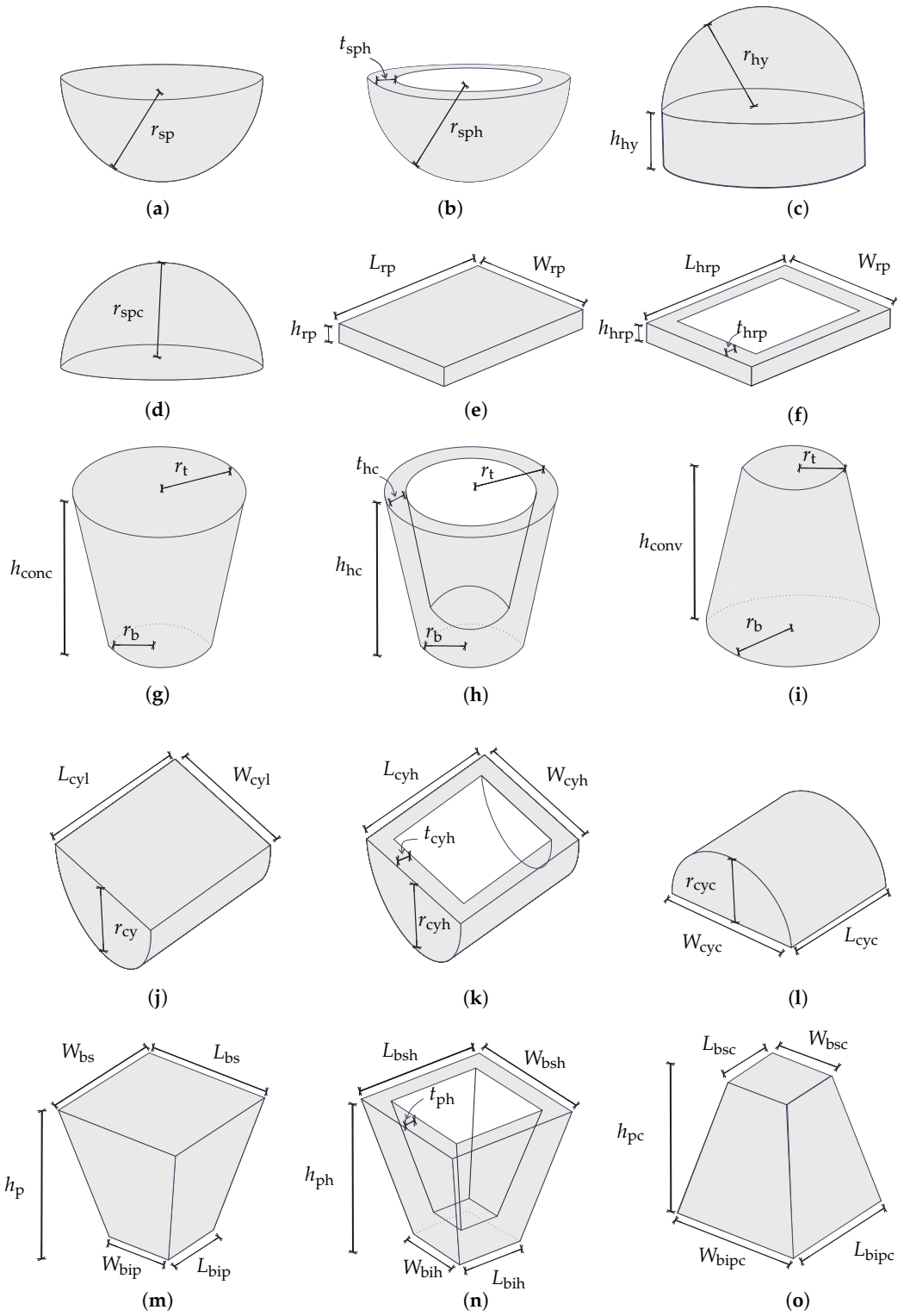


Figure 2. Geometric shapes for the resonator considered in this study: (**a**) concave hemisphere; (**b**) hollow concave hemisphere; (**c**) cylindrical hemisphere; (**d**) hemisphere; (**e**) rectangular prism; (**f**) hollow rectangular prism; (**g**) inverted cone; (**h**) hollow inverted cone; (**i**) cone; (**j**) inverted half-cylinder; (**k**) hollow inverted half-cylinder; (**l**) half-cylinder; (**m**) inverted trapezoidal prism; (**n**) hollow inverted trapezoidal prism; and (**o**) trapezoidal prism.

A brief description of the aforementioned geometric shapes is provided below.

- Cap-based geometries: Cap-based geometries are highly effective for confining and controlling electromagnetic energy due to their curved shapes, which minimize energy losses by reducing surface currents. These geometries facilitate the design of compact resonators with high-quality factor Q, characterized by sharp and selective frequency responses. Additionally, cap-based resonators can enhance antenna BW and support multiple modes, including TE, TM, and whispering gallery (WG) modes, making them versatile for various RF applications. Cap-based resonators can be constructed from dielectric or metallic materials, offering a favorable trade-off between performance and size. Dielectric materials provide strong field confinement and compact designs, while metallic structures ensure a high Q factor by minimizing energy dissipation. However, the performance of these resonators is sensitive to minor geometric deviations, which can lead to frequency shifts and degraded Q factor. Materials with low thermal expansion coefficients are essential to maintain frequency stability, particularly in high-precision applications. In this work, we focus on designing resonators using the following cap-based geometries: Figure 2a concave hemisphere, Figure 2b hollow concave hemisphere, Figure 2c cylindrical hemisphere, and Figure 2d hemisphere. Each geometry is tailored to specific performance needs. The cylindrical hemisphere offers superior coupling and broader BW, making it ideal for applications requiring enhanced interaction with the patch antenna. The concave hemisphere improves gain and radiation directionality, making it suitable for gain-critical designs. The hollow concave hemisphere achieves the best trade-off between maximum gain, efficiency, and BW due to its strong field confinement and reduced material losses, although it presents greater fabrication complexity. Lastly, the hemisphere provides a simple, cost-effective solution for narrow-band applications, where moderate gain and efficiency are sufficient [33,34].
- Rectangular prism-based geometries: Rectangular prism-based geometries are widely used for their simplicity, robust design, and predictable performance. These geometries confine electromagnetic waves, making them ideal for compact and reliable resonators. They support TE and TM modes, with the resonant frequency determined by their physical dimensions. Their fabrication is straightforward, utilizing standard machining or dielectric molding methods. Typically, they are constructed from high-dielectric-constant materials, which enable a significant reduction in resonator size. Furthermore, these geometries exhibit a high quality factor (Q), resulting in minimal energy loss and ensuring sharp and selective frequency responses. Despite these advantages, rectangular prism-based resonators have some drawbacks. They require materials with low thermal expansion coefficients to maintain frequency stability and their design must carefully isolate the desired mode to avoid interference from unwanted modes. In this work, we focus on designing resonators using the following rectangular prism-based geometries: Figure 2e rectangular prism and Figure 2f hollow rectangular prism. Note that the hollow rectangular prism helps provide better mode control, broader BW, high efficiency, and reduced weight but is more complex to fabricate and requires careful design to suppress unwanted modes. Conversely, the rectangular prism is well-suited for antenna designs requiring simplicity, small size, reduced energy loss, and a high Q factor, particularly in narrowband applications [19,35,36].
- Cone-based geometries: Cone-based geometries utilize conical shapes to effectively confine and control electromagnetic energy. These geometries have an intrinsic ability to suppress and mitigate unwanted higher-order modes due to the natural tapering of the cone, which reduces interference and enhances frequency selectivity. The field confinement near the cone apex is excellent, making this geometry ideal for achieving

high Q factors and precise frequency responses. Furthermore, cone-based designs result in compact resonators, which are well-suited for improving radiation efficiency and BW. Despite these advantages, cone-based geometries present challenges in fabrication. The precision required to manufacture the tapering shape is critical, particularly for high-frequency applications. Additionally, materials with low thermal expansion coefficients are essential to maintain frequency stability under varying environmental conditions. In this work, we focus on designing resonators using the following cone-based geometries: Figure 2g inverted cone, Figure 2h hollow inverted cone, and Figure 2i cone. Each geometry serves specific performance goals. The hollow inverted cone is particularly beneficial when gain, BW, and weight reduction are critical; however, it is more complex to design and fabricate due to its hollow structure. The inverted cone is advantageous for improving BW and efficiency, as its geometry provides better coupling with the patch antenna. Lastly, the cone offers a simple and compact resonator design suitable for applications with sufficient moderate performance improvements [22,37].

- Half-cylinder-based geometries: Half-cylinder-based geometries are highly effective for enhancing the performance of patch antennas, particularly in terms of gain, BW, and efficiency. The curved surface of the half-cylinder provides excellent field confinement, especially near the apex, while the flat surface improves coupling and integration with the patch antenna. This combination enhances the radiation efficiency and directional properties of the antenna, making these geometries suitable for a wide range of applications. Additionally, their compact form factor makes them ideal for space-constrained designs. These geometries support TE and TM modes and offer better mode isolation and control than other designs. The resonance characteristics are determined by the physical dimensions of the half-cylinder, which directly influence its performance. As a result, they are well-suited for wideband patch antennas, where BW and efficiency are critical. However, there are challenges associated with half-cylinder-based geometries. Achieving precise dimensions and smooth surfaces is crucial to maintaining consistent resonant characteristics, especially at high frequencies, where minor deviations can degrade performance. Furthermore, materials with low thermal expansion coefficients must ensure frequency stability under varying environmental conditions. In this work, we focus on designing resonators using the following half-cylinder-based geometries: Figure 2j inverted half-cylinder, Figure 2k hollow inverted half-cylinder, and Figure 2l half-cylinder. The inverted half-cylinder is handy when strong coupling and wide BW are required, balancing performance and moderate fabrication complexity. A hollow inverted half-cylinder is the most suitable choice for applications with critical gain, BW, and weight reduction. However, it poses more significant challenges in fabrication due to its intricate structure. Lastly, the half-cylinder is a cost-effective option for narrowband applications requiring moderate performance improvements and simplicity in design [19].
- Trapezoidal prism-based geometries: Trapezoidal prism-based geometries are highly appealing for achieving effective field confinement, mode control, and design adaptability. The slanted sides and non-uniform cross-section significantly alter the electromagnetic field distribution, making these geometries highly efficient for compact antennas with enhanced gain and BW. The tapering structure improves coupling with patch antennas by reducing reflections and minimizing energy losses, broadening operational BW. Additionally, these geometries support TE and TM modes while inherently suppressing higher-order modes, leading to cleaner and more stable frequency responses. Precision in fabrication is required for trapezoidal prism-based geometries, particularly at higher frequencies, where minor dimensional inaccura-

cies can degrade performance. Thermal stability is another important consideration, as materials with low thermal expansion coefficients are required to ensure consistent performance under varying environmental conditions. In this work, we focus on designing resonators using the following trapezoidal prism-based geometries: Figure 2m inverted trapezoidal prism, Figure 2n hollow inverted trapezoidal prism, and Figure 2o trapezoidal prism. The inverted trapezoidal prism offers improved coupling and broader BW due to its optimized field distribution, making it suitable for wideband applications with moderate fabrication complexity. The hollow inverted trapezoidal prism is the most appropriate choice when maximum gain, BW, and weight reduction are required. Its hollow structure maintains strong electromagnetic confinement while minimizing material losses, although it poses more significant challenges in fabrication. Lastly, the trapezoidal prism is an effective and cost-efficient option for narrowband applications, offering simplicity in design and fabrication alongside moderate performance improvements [38].

Finally, a comprehensive comparison of these geometries is provided in Table 2, highlighting their distinct characteristics and suitability for various design applications.

Table 2. Comparison between the chosen geometries for designing RF resonators applied to improve patch antennas.

Feature	Cap-Based	Rectangular Prism-Based	Cone-Based	Half-Cylinder-Based	Trapezoidal Prism-Based
Field Confinement	Strong due to curved shapes, minimizing surface currents.	Strong, confined throughout the solid volume; highly dependent on material properties.	Strong near the apex, with an efficient energy focus.	Strong along the curved surface; excellent near the apex of the curve.	Concentrated in specific regions due to tapering and slanted sides.
Mode Control	Supports TE, TM, and WG modes with good isolation; susceptible to higher-order modes.	Good for TE and TM modes; requires optimization to suppress unwanted modes.	Efficient mode isolation; higher-order modes naturally suppressed by tapering shape.	Improved suppression of higher-order modes due to curved surface design.	Excellent suppression of higher-order modes due to the non-uniform cross-section.
Bandwidth	Moderate to wide, depending on geometry (e.g., hollow concave geometries offer the broadest BW).	Moderate; limited by material losses in solid structures.	Wide, especially with hollow designs.	Moderate to wide, depending on fabrication and material choices.	Broad, enhanced by tapering sides and minimized reflections.
Gain	Improved for concave and hollow concave designs; uniform for hemispheres.	Moderate; enhanced by compact designs and high-dielectric materials.	High, particularly for hollow cones focusing energy efficiently.	High, with directional improvements due to curved surfaces.	High, with enhanced directionality from slanted sides and tapering structure.
Radiation Efficiency	Enhanced for hollow and concave geometries due to reduced losses.	Moderate; heavily influenced by dielectric or metallic material properties.	High, due to focused field confinement near the apex.	High, particularly for inverted configurations that improve coupling.	High, with improved coupling from the slanted sides.
Compactness	Compact, especially for dielectric-based designs.	Compact and straightforward; solid structures are space-efficient.	Compact due to tapering design; hollow structures reduce size further.	Compact, particularly for standard half-cylinders; slightly larger for hollow designs.	Compact, with efficient utilization of space due to slanted sides.
Fabrication Complexity	Moderate to high, especially for hollow and concave geometries requiring precision.	Low; straightforward to machine or mold.	Moderate to high, with tapering and hollow structures requiring precision.	Moderate; requires precision for curved surfaces and hollow configurations.	Moderate to high; precise fabrication of slanted sides and tapering required.
Thermal Stability	Requires low thermal expansion materials for high-frequency stability.	Good for solid designs; dependent on material properties.	Dependent on material selection; hollow designs may introduce stability concerns.	Requires low-expansion materials for consistent performance.	Dependent on material properties; precision is critical at high frequencies.
Applications	Wideband systems (e.g., hollow concave), gain-critical designs (e.g., concave), or narrowband (hemisphere).	Narrowband filters, high-Q resonators, and compact antenna designs.	Wideband, high-gain applications, and systems requiring focused field confinement.	Gain-critical systems, wideband applications (inverted or hollow), and compact designs.	Wideband, high-gain systems, and compact or weight-sensitive designs.

4. Analysis of Numerical Results

In this section, we analyze the results of numerical simulations conducted to design resonators using a combination of fifteen geometric shapes and three materials, as detailed in Section 3, to enhance the performance of a probe-fed patch antenna. Following the decoupled method, the probe-fed patch antenna is designed first, and the resonator is subsequently introduced to improve its performance. For making the comparisons clear, the $|S_{11}|$ and radiation pattern plots include results from the probe-fed patch antenna obtained with and without the resonator.

The numerical simulations were conducted using the Microwave & RF package of Computer Simulation Technology (CST) software [39] release Version 2023.0. The computational setup consisted of an Intel Core i7 processor (2.10 GHz clock speed) Intel Corporation, Santa Clara, USA with 32 GB of RAM. The simulation time for each antenna geometry ranged from 8 to 72 h, depending on the complexity of the structure. Regarding the simulation, we point out the following factors that influence the simulation time:

- Solver choice: The frequency-domain (FD) and time-domain (TD) solvers have different computational requirements. The TD solver generally require more memory; however, it enable faster broadband analysis. This solver is preferred for simulating the interaction between an antenna and a resonator because it provides a broadband response in a single simulation, making it more efficient for complex geometries. It facilitates the analysis of coupling, S-parameters, and transient response. The FD solver, conversely, is better for specific frequencies and dispersive materials. Therefore, the TD solver was chosen for this work, as it is well-suited for simulating antennas and resonators, providing efficient broadband analysis in a single simulation.
- Mesh refinement: A finer mesh improves accuracy but significantly increases memory usage and CPU time. In many cases, a mesh convergence study is recommended to find a suitable balance between accuracy and efficiency. In the simulations with graphite, it was necessary to gradually reduce the mesh due to long simulation times and memory errors. The reduction was made carefully to maintain the accuracy of the results, while balancing computational efficiency. This approach allowed the simulations to run without compromising the quality of the results.
- Boundary conditions: For simulating antennas and resonators in CST, the ideal boundary conditions depend on the simulation setup. An electric perfect conductor is best for metal structures, as it establishes a perfect conductor boundary. A magnetic perfect conductor can be used in specific cases involving magnetic resonance or properties. For symmetrical structures, electric/magnetic symmetry can reduce computation time. Open (Add Space) with perfectly matched Layers (PML) is recommended for free-space simulations, as it absorbs outgoing waves, preventing reflections. Generally, Open (Add Space) is the preferred condition for antenna and resonator simulations in open environments. Therefore, in our simulations, we opted for the Open (Add Space) boundary condition.
- Material properties: Complex materials, such as dispersive or lossy media, require additional computations to accurately model their behavior. This increases processing time, as the solver must handle complex equations to account for absorption and dispersion effects. In this study, DW and glycerin moderately extend simulation time due to their high permittivity, while graphite, being highly conductive, has a much greater impact on computation time.
- Resonator complexity: Complex resonator shapes and material combinations directly impact computational load, as these geometries require finer meshing to maintain simulation accuracy. Additionally, solver convergence may take longer, as intricate structures often need more iterations to reach a stable solution. We analyzed different

materials and geometric shapes and observed that some geometries required significantly more time to simulate. Among the materials tested, graphite took the longest to simulate, followed by glycerin and DW, respectively.

The probe-fed patch antenna is mounted on an FR-4 substrate, characterized by $\varepsilon_r = 4.5$ and $\tan\delta = 0.013$, $\mu_r = 1$, and operates at a resonant frequency of $f_r = 2.45$ GHz. Figure 3 illustrates the probe-fed patch antenna, which has dimensions of $L = 28.83$ mm and $W = 15.00$ mm, with the probe-fed point located 9.61 mm from the lower edge and 7.50 mm from the side edges.

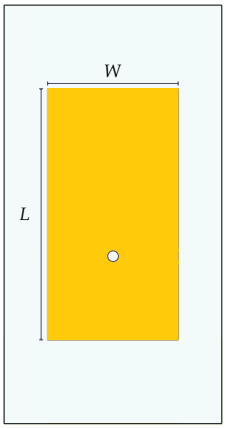


Figure 3. The probe-fed patch antenna.

The resonator is positioned above the radiating element of the probe-fed patch antenna, with its bottom center aligned with the center of the radiator. For cylindrical and prism-shaped geometries, alignment can occur along either LPA or WPA, where LPA refers to the resonator's length aligned with the patch antenna's length, and WPA refers to the resonator's length aligned with the patch antenna's width. To evaluate the effects of these configurations, specific dimensions of the geometric shapes were varied to assess their influence on performance. The chosen dimensions and their variation ranges are provided in Appendix A. Moreover, the key properties of the DW, glycerin, and graphite materials used in the resonators are summarized in Table 3.

Table 3. Material properties used in the numerical simulations.

Material	ε_r	μ_r	σ (S/m)
DW	78.4	1	5.55 µ
Glycerin	50	1	0
Graphite	12	1	100 k

The performance comparison among the combinations primarily relies on the radiation pattern and the magnitude of the scattering parameter S_{11} ($|S_{11}|$). We conducted the numerical simulations under identical conditions and parameters. Additionally, we assume that an acceptable value for $|S_{11}|$ is below -10 dB. Consequently, the BW of the overall patch antenna is defined as the frequency BW around f_r that satisfies this criterion. All reported numerical results consider the resonator with dimensions varying within the intervals and resolutions listed in Table A1 in Appendix A. Moreover, the discussed numerical results correspond to the highest value of the MLM, where MLM represents the realized gain. The radiation patterns in polar form at a frequency of 2.45 GHz were analyzed at an azimuth angle of $\phi = 0°$, with the elevation angle varying from $\theta = 0°$ to $\theta = 360°$.

This section is organized as follows: Section 4.1 addresses the resonator based on DW, Section 4.2 addresses the resonator based on glycerin, Section 4.3 addresses the resonator based on graphite, and Section 4.4 provides general discussions about the numerical results obtained with the considered materials.

4.1. Distilled Water Resonator

This subsection evaluates the performance of various geometric shapes for the DW resonator. The $|S_{11}|$ parameter for the cap-based, rectangular prism-based, cone-based, half-cylinder-based, and trapezoidal prism-based geometries are shown in Figure 4a, Figure 4b, Figure 4c, Figure 5a, and Figure 5b, respectively. Furthermore, the radiation patterns for the cap-based, rectangular prism-based, cone-based, half-cylinder-based, and trapezoidal prism-based geometries are illustrated in Figure 6a, Figure 6b, Figure 6c, Figure 7a, and Figure 7b, respectively. Moreover, Table 4 summarizes key parameter values obtained at the resonant frequency.

Regarding cap-based geometries, $|S_{11}|$ in Figure 4a show that the concave hemisphere and hemisphere geometries exhibit additional notches, indicating multiple impedance matching points. These notches suggest the patch antenna can operate at multiple resonant frequencies, offering enhanced potential for multi-band propagation. Among the cap-based geometries, the cylindrical hemisphere achieves the broadest BW, as detailed in Table 4, offering an extended frequency range for enabling impedance matching. Concerning the radiation pattern, shown in Figure 6a, the concave hemisphere achieves the highest MLM value. At the same time, the cylindrical hemisphere and hollow concave hemisphere also exhibit MLM values exceeding that of the patch antenna without a resonator. Additionally, a significant variation in MLD is observed in the hemisphere geometry, altering MLD values from 0° to 135° and leading to a performance reduction. As listed in Table 4, all cap-based geometries presented a decrease in HPBW and SLL, with the cylindrical hemisphere being an exception in terms of SLL.

Considering rectangular prism-based geometries, the $|S_{11}|$ shown in Figure 4b demonstrate distinct performances. For instance, the rectangular prism maintains an acceptable $|S_{11}|$ and provides a BW comparable to the patch antenna without a resonator. In contrast, the hollow rectangular prism exhibits unacceptable $|S_{11}|$ limits. Concerning the radiation pattern, as shown in Figure 6b, the rectangular prism achieves the highest MLM value, whereas the hollow rectangular prism displays the lowest MLM value compared to the patch antenna without a resonator. Furthermore, as summarized in Table 4, the rectangular prism reduces the HPBW, while the hollow rectangular prism increases it. Additionally, the SLL is maintained for the rectangular prism but reduced for the hollow rectangular prism compared to the patch antenna without a resonator.

Regarding the findings for cone-based geometries, all exhibit acceptable $|S_{11}|$ values, as depicted in Figure 4c. The cone achieves the highest BW, while the inverted and hollow inverted cones display the most favorable $|S_{11}|$. In terms of the radiation pattern, Figure 6c, the inverted cone achieves the highest MLM value, followed by the hollow inverted cone. Moreover, all cone-based geometries achieve MLM values higher than the patch antenna without a resonator. Both the inverted cone and hollow inverted cone show reductions in HPBW and SLL compared to the patch antenna without a resonator, Figure 6c and Table 4, and, consequently, they enhance the directionality of the patch antenna.

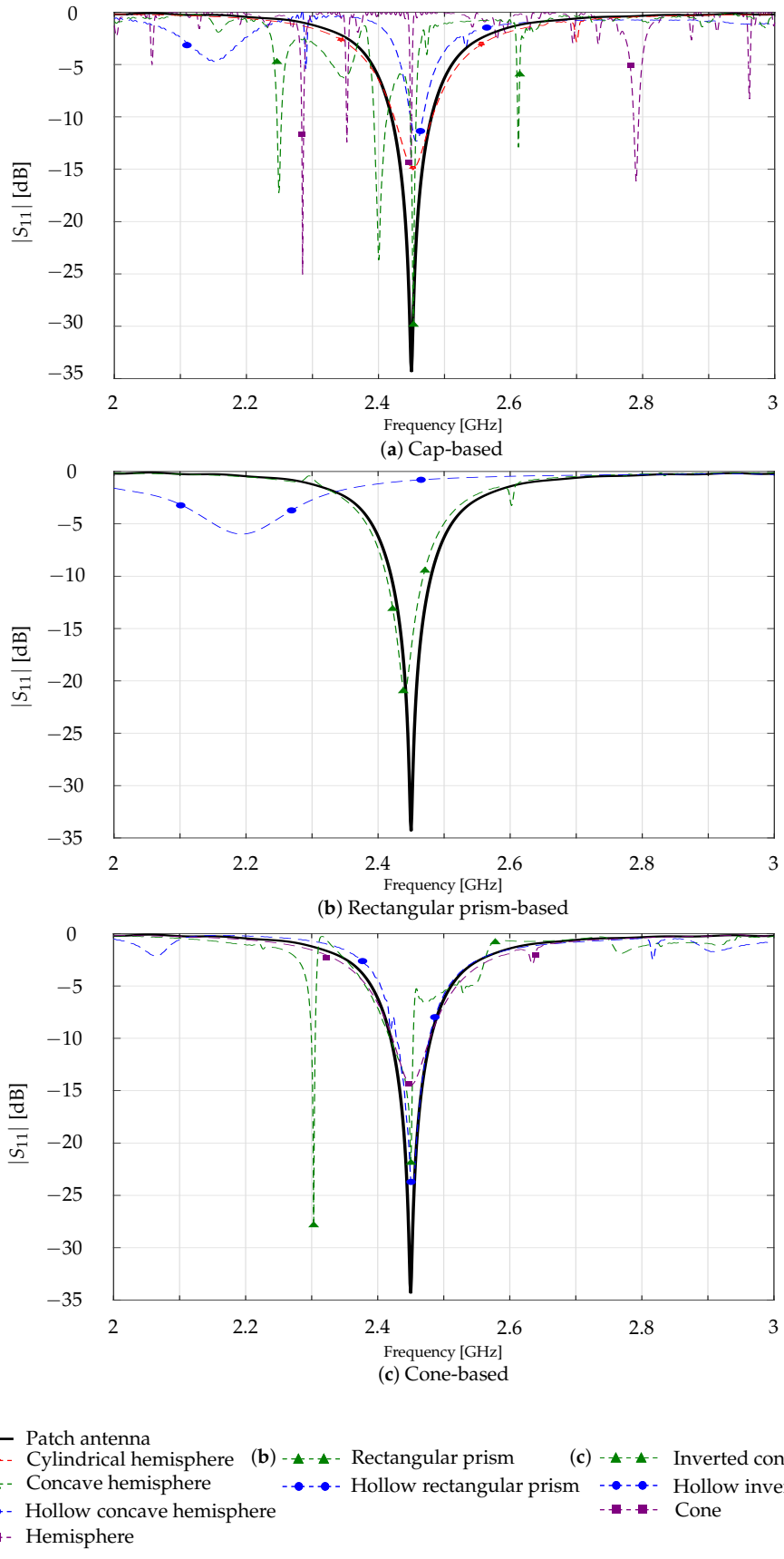


Figure 4. Patch antenna with a DW-made resonator: magnitude of the scattering parameter ($|S_{11}|$). (**a**) cap-based; (**b**) rectangular prism-based; and (**c**) cone-based.

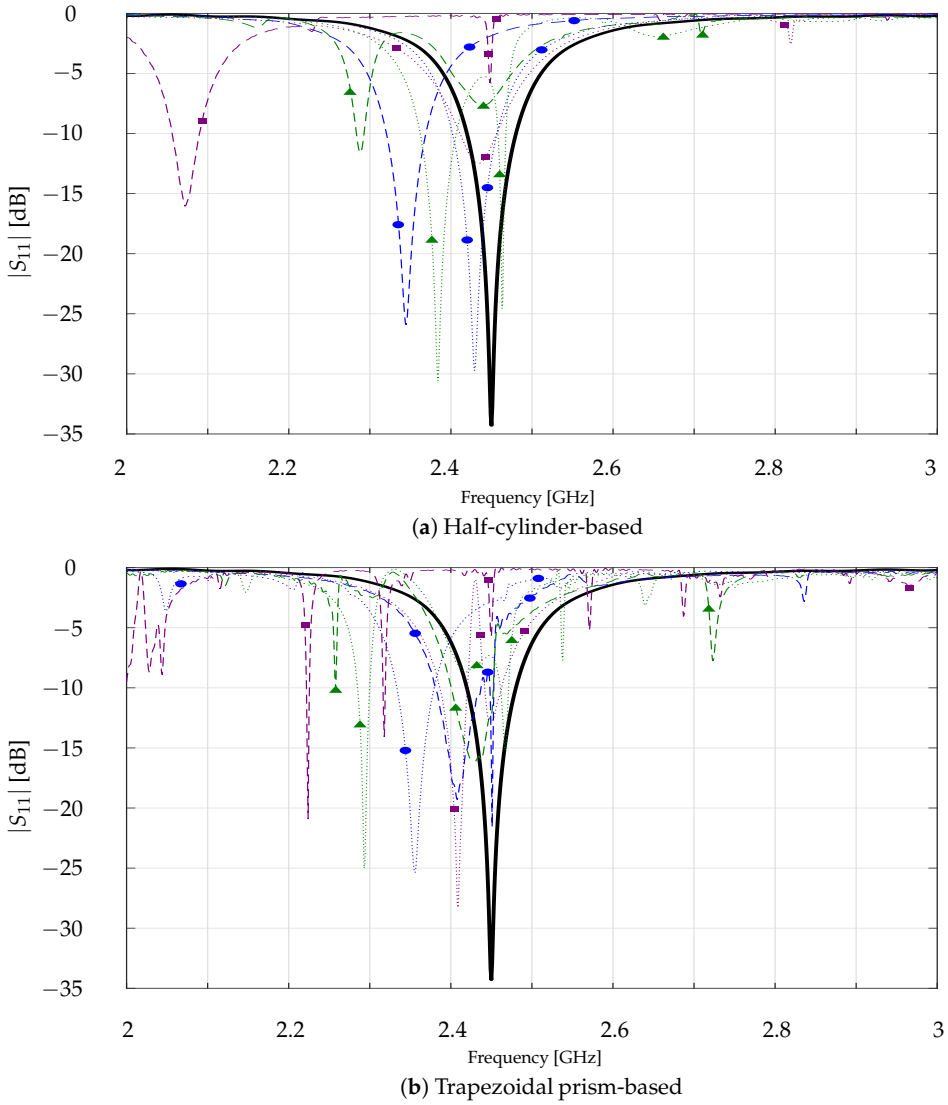
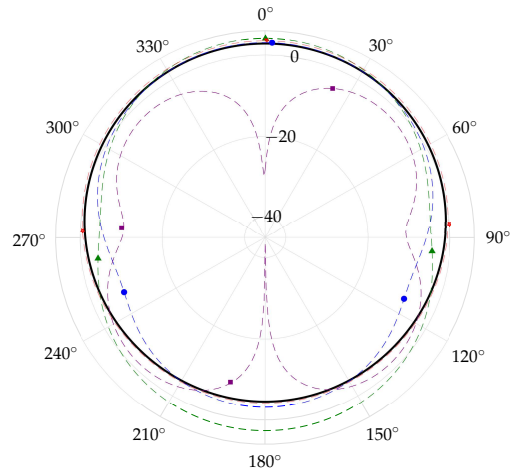
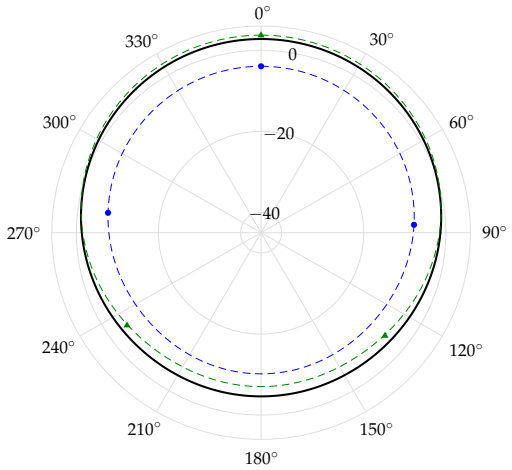


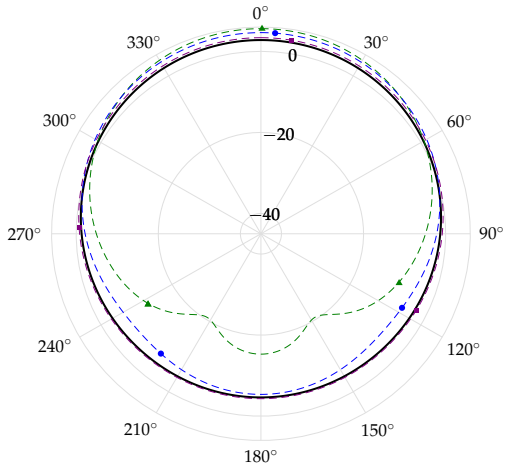
Figure 5. Patch antenna with a DW-made resonator: magnitude of the scattering parameter ($|S_{11}|$). (**a**) half-cylinder-based; and (**b**) trapezoidal prism-based.



(**a**) Cap-based



(**b**) Rectangular prism-based



(**c**) Cone-based

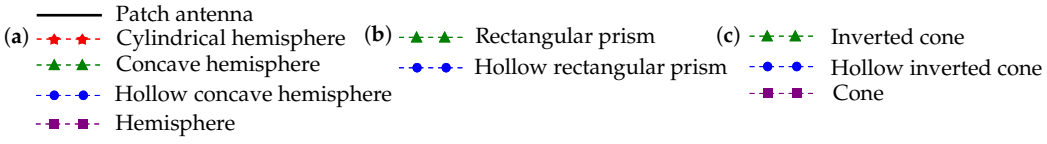
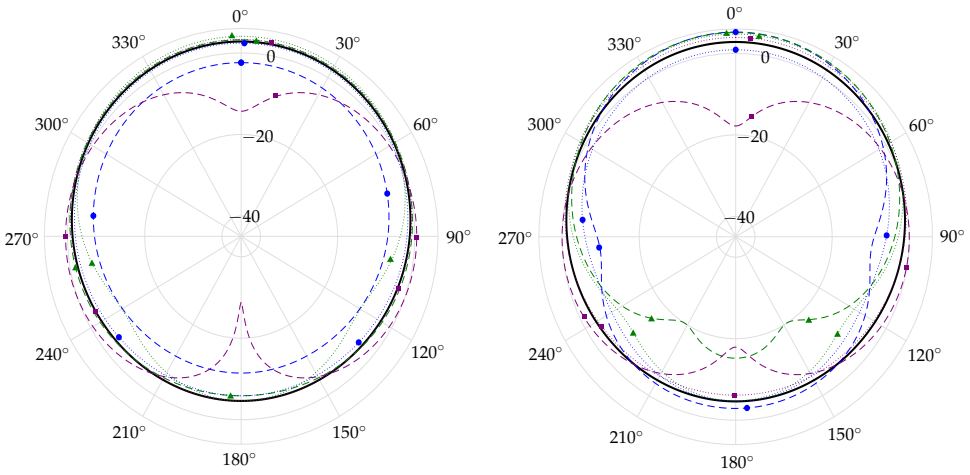


Figure 6. Patch antenna with a DW-made resonator: the radiation pattern plot of the 1D far-field realized gain ($\phi = 0$). (**a**) cap-based; (**b**) rectangular prism-based; and (**c**) cone-based.



(**a**) Half-cylinder-based (**b**) Trapezoidal prism-based

Figure 7. Patch antenna with a DW-made resonator: the radiation pattern plot of the 1D far-field realized gain ($\phi = 0$). (**a**) half-cylinder-based; and (**b**) trapezoidal prism-based.

Table 4. Patch antenna with a DW-made resonator: Key parameters values at the resonant frequency.

Geometry	$\lvert S_{11}\rvert$ (dB)	BW (MHz)	MLM (dBi)	HPBW (°)	SLL (dB)
Patch antenna	−34.30	60	2.79	148.2	w/o
Rectangular prism	−17.03	55	3.73	132.4	w/o
Hollow rectangular prism	−0.86	w/o	−3.94	151.4	−6.2
Cylindrical hemisphere	−14.82	57	3.39	142.6	w/o
Concave hemisphere	−14.46	29.04	4.1	88.1	−1.4
Hollow concave hemisphere	−10.57	18	3.04	111.4	−6.2
Hemisphere	−12.41	1	−1.46	48.5	−1
Inverted cone	−22.06	34	5.6	95.4	−20.9
Hollow inverted cone	−23.50	49	4.62	119.8	−10
Cone	−14.44	55	3.37	147	w/o
LPA Inverted half-cylinder	−7.28	w/o	3.21	148.4	w/o
LPA hollow inverted half-cylinder	−1.85	w/o	−2.39	139.6	w/o
LPA half-cylinder	−4.04	w/o	0.49	w/o	w/o
WPA inverted half-cylinder	−5.90	16	4.07	116.7	−8.8
WPA hollow inverted half-cylinder	−12.26	54	2.38	143	w/o
WPA half-cylinder	−11.02	44	3.32	144.7	w/o
LPA inverted trapezoidal prism	−12.44	51	5.12	104.5	−20.3
LPA hollow inverted trapezoidal prism	−16.10	52	5.22	85.7	−8.1
LPA trapezoidal prism	−5.72	w/o	−0.02	84	w/o
WPA inverted trapezoidal prism	−7.47	9	4.73	117.2	−9.5
WPA hollow inverted trapezoidal prism	−2.87	w/o	0.89	119.5	−5.4
WPA trapezoidal prism	−12.65	40	3.9	133.7	w/o

The results for the half-cylinder-based geometries reveal that the WPA inverted half-cylinder, as shown in Figure 5a, exhibits additional notches in $\lvert S_{11}\rvert$, enabling multiple resonant frequencies. Moreover, all LPA half-cylinder shapes reduce the resonant frequency, indicating their potential for reducing the patch antenna size. The WPA inverted hollow

half-cylinder also presents a BW close to the patch antenna without a resonator. For the radiation pattern, as illustrated in Figure 7a and summarized in Table 4, the WPA and LPA inverted half-cylinders and WPA half-cylinder achieve MLM values higher than the patch antenna without resonator. The WPA inverted half-cylinder significantly enhances directionality, achieving substantial reductions in both HPBW and SLL compared to the patch antenna without a resonator. Moreover, the LPA half-cylinder geometry causes a notable alteration in MLD, changing its value from 0° to 90°, resulting in a decline in performance.

Finally, for trapezoidal prism-based geometries, it is evident that most of these geometries reveal additional notches in $|S_{11}|$, enabling multiple resonant frequencies, except for the WPA hollow inverted trapezoidal prism, shown in Figure 5b. Furthermore, all trapezoidal prism-based geometries show potential for antenna size reduction at lower frequencies, particularly with the LPA half-cylinder. Moreover, the BW values for the LPA inverted and hollow inverted trapezoidal prisms are the highest and comparable to the patch antenna without a resonator, as presented in Table 4. Concerning the radiation pattern, depicted in Figure 7b and detailed in Table 4, the LPA hollow inverted and inverted trapezoidal prisms, followed by the WPA inverted trapezoidal prism and trapezoidal prism, exhibit significant improvements in terms of MLM. Note that all these geometries achieve reductions in terms of HPBW, with the LPA trapezoidal prism, hollow inverted, and inverted trapezoidal prisms achieving the highest reductions in this order. Most of the trapezoidal prism-based geometries also present reductions in SLL, particularly the LPA inverted trapezoidal prism. These characteristics lead to enhanced directionality and improved efficiency.

Overall, the analysis of the different geometric shapes for the DW resonator reveals notable differences in performance. The cap-based and trapezoidal prism-based geometries are capable of achieving multiple resonant frequencies. Additionally, LPA half-cylinder shapes and trapezoidal prism-based geometries show potential for reducing the patch antenna size. Analyzing the results at the resonant frequency, Table 4, cone-based geometries exhibit the best performance. Regarding BW, the cylindrical hemisphere exhibits the highest value, followed by rectangular prism and cone. Regarding radiation pattern, the inverted cone achieves the most significant improvement in terms of MLM, along with substantial reductions in HPBW and SLL, which enhance the directionality of the patch antenna. Similarly, the LPA hollow inverted and inverted trapezoidal prism geometries exhibit comparable improvements, reinforcing their suitability for efficient and directional antenna designs. For consistency across the tables, 'w/o' is used to denote 'without', meaning that the parameter is either not applicable or was not detected in the evaluated scenarios.

4.2. Glycerin Resonator

In this subsection, we explore the integration of glycerin resonators into the patch antenna by evaluating the performance of different geometric shapes. The $|S_{11}|$ parameter for cap-based, rectangular prism-based, cone-based, half-cylinder-based, and trapezoidal prism-based geometries are shown in Figure 8a, Figure 8b, Figure 8c, Figure 9a, and Figure 9b, respectively. Furthermore, the corresponding radiation patterns for cap-based, rectangular prism-based, cone-based, half-cylinder-based, and trapezoidal prism-based geometries are shown in Figure 10a, Figure 10b, Figure 10c, Figure 11a, and Figure 11b, respectively. Moreover, Table 5 lists key parameter values obtained at the resonant frequency.

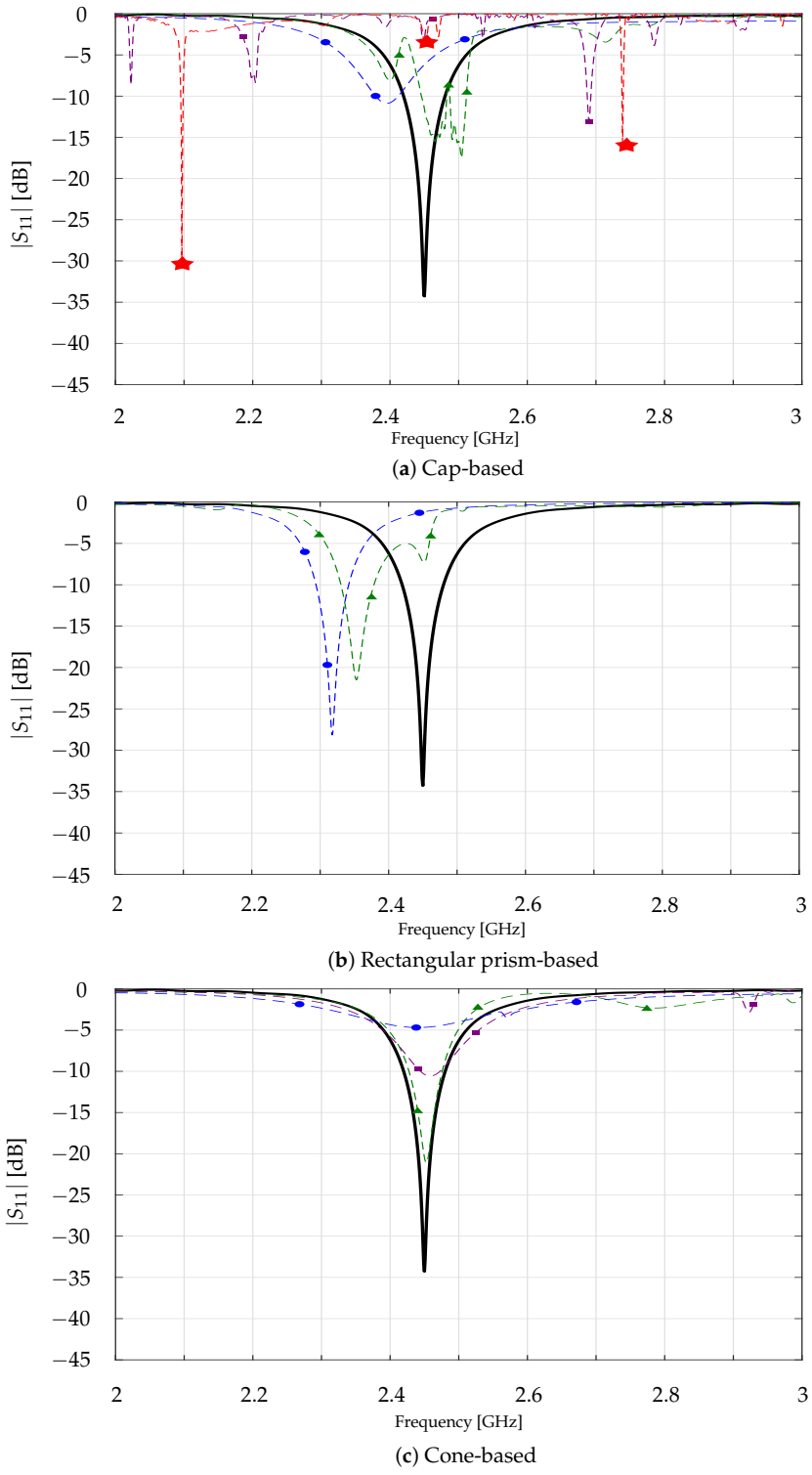


Figure 8. Patch antenna with a glycerin-made resonator: magnitude of the scattering parameter ($|S_{11}|$). (**a**) cap-based; (**b**) rectangular prism-based; and (**c**) cone-based.

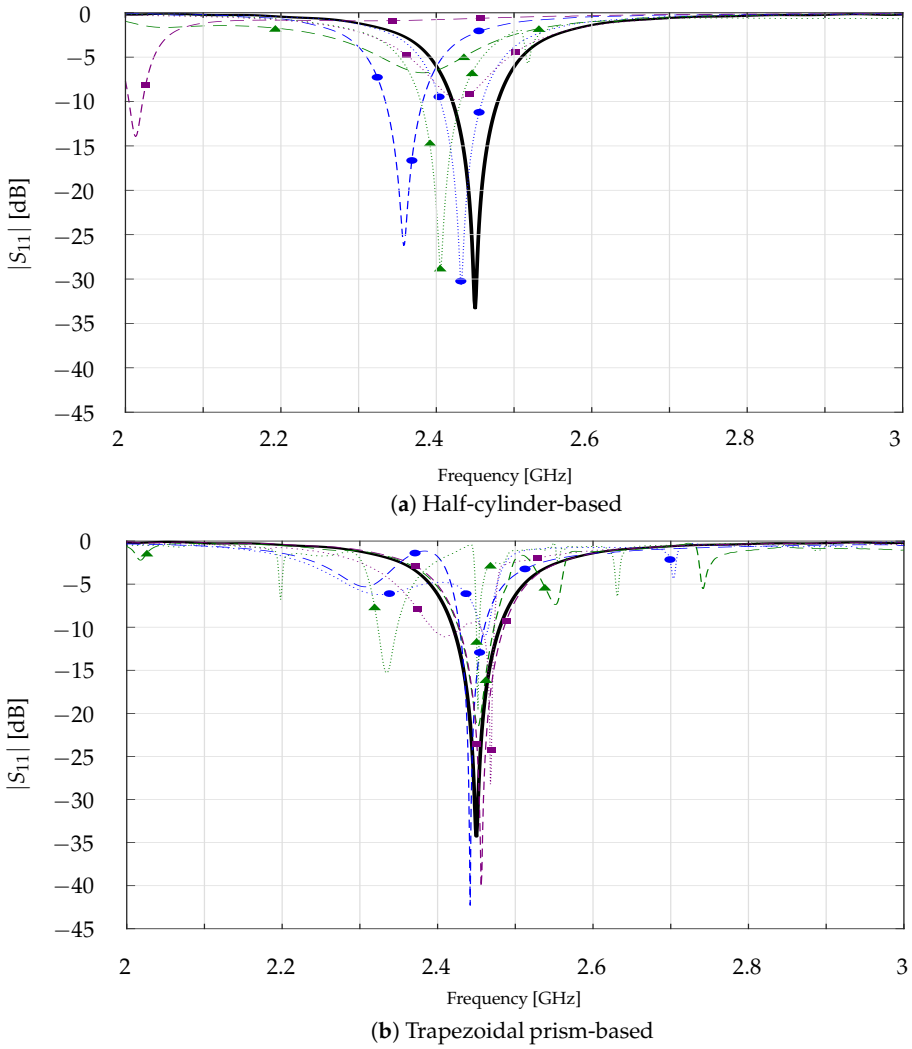
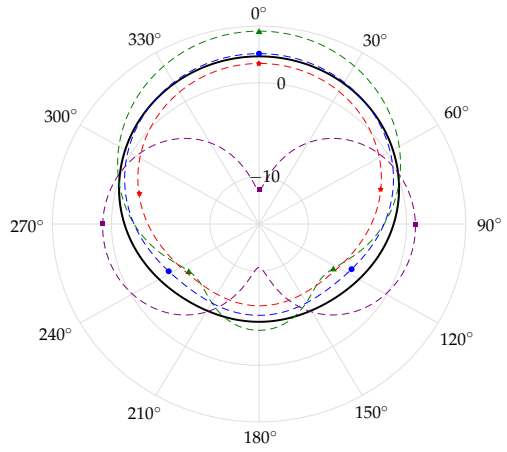
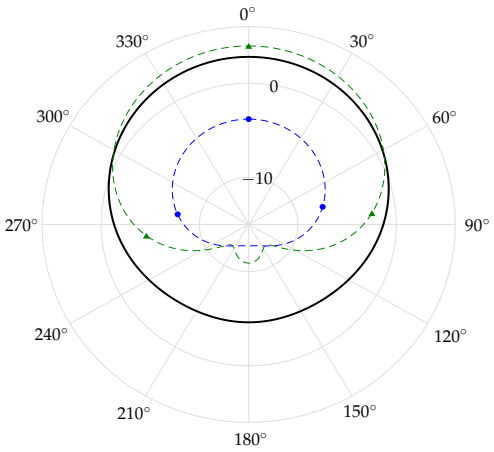


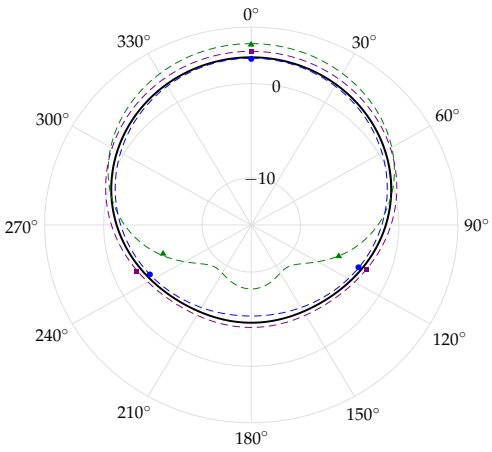
Figure 9. Patch antenna with a glycerin-made resonator: magnitude of the scattering parameter ($|S_{11}|$). (**a**) half-cylinder-based; and (**b**) trapezoidal prism-based.



(**a**) Cap-based



(**b**) Rectangular prism-based



(**c**) Cone-based

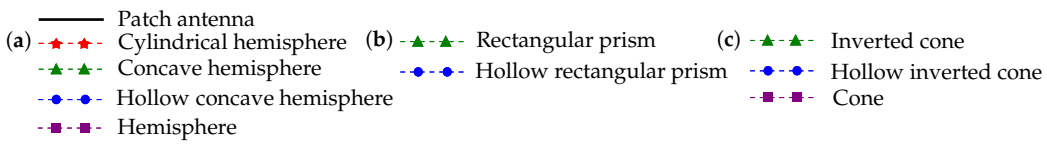


Figure 10. Patch antenna with a glycerin-made resonator: the radiation pattern plot of the 1D far-field realized gain ($\phi = 0$). (**a**) cap-based; (**b**) rectangular prism-based; and (**c**) cone-based.

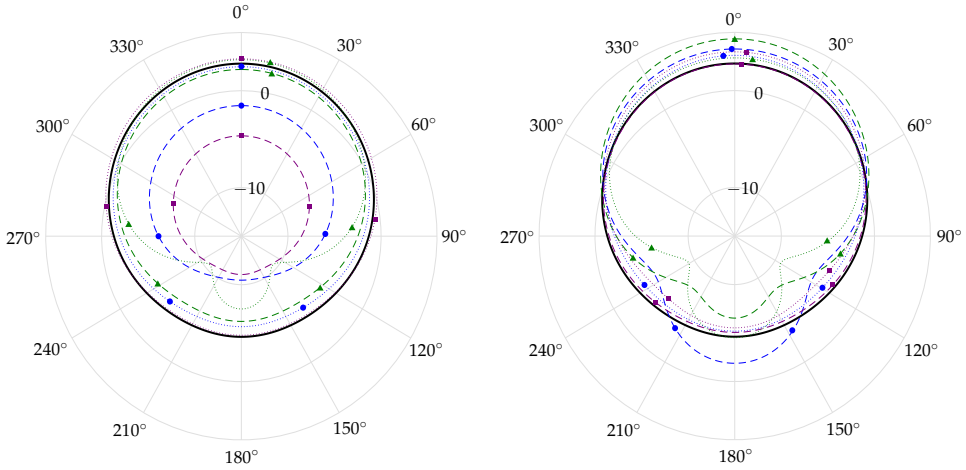


Figure 11. Patch antenna with a glycerin-made resonator: the radiation pattern plot of the 1D far-field realized gain ($\phi = 0$). (**a**) half-cylinder-based; and (**b**) trapezoidal prism-based.

Table 5. Patch antenna with a glycerin-made resonator: Key parameters values at the resonant frequency.

Geometry	$\lvert S_{11}\rvert$ (dB)	BW (MHz)	MLM (dBi)	HPBW (°)	SLL (dB)
Patch antenna	−34.30	60	2.79	148.2	w/o
Rectangular prism	−7.24	w/o	3.95	117.2	−14.9
Hollow rectangular prism	−1.21	w/o	−3.82	140.5	w/o
Cylindrical hemisphere	−3.72	w/o	2.04	120.2	-8.4
Concave hemisphere	−11.48	54	5.46	101.8	−9.2
Hollow concave hemisphere	−6.19	11	3.08	127.3	−8.4
Hemisphere	−3.27	w/o	0.89	91	w/o
Inverted cone	−21.08	47	4.24	125.2	−12.4
Hollow inverted cone	−4.68	w/o	2.69	139.1	w/o
Cone	−10.57	27	3.42	146.9	w/o
LPA Inverted half-cylinder	−4.39	w/o	2.18	139.2	w/o
LPA hollow inverted half-cylinder	−2.34	w/o	−1.54	140.7	w/o
LPA half-cylinder	−0.66	w/o	−4.65	152.4	−6.4
WPA inverted half-cylinder	−6.30	32	3.19	120.5	−10.7
WPA hollow inverted half-cylinder	−13.56	54	2.47	143.5	w/o
WPA half-cylinder	−8.95	8	3.28	144	w/o
LPA inverted trapezoidal prism	−21.20	45	5.33	104.1	−11.9
LPA hollow inverted trapezoidal prism	−15.98	31	4.28	117.7	−6.2
LPA trapezoidal prism	−22.81	57	2.74	145.6	w/o
WPA inverted trapezoidal prism	−10.30	3	3.37	120.9	−7.9
WPA hollow inverted trapezoidal prism	−8.44	9	3.63	119.8	w/o
WPA trapezoidal prism	−9.33	17	3.99	118.6	−9.5

The evaluation of the cap-based geometries reveals distinct characteristics in both $\lvert S_{11}\rvert$ and radiation pattern as illustrated in Figure 8a and Figure 10a, respectively. The cylindrical hemisphere geometry reduces the resonant frequency, showing its potential for reducing

the patch antenna size, and introduces multiple resonant frequencies. Conversely, the hemisphere geometry increases the resonant frequency, which can be advantageous for applications requiring higher operating frequencies. In terms of BW, as listed in Table 5, the concave hemisphere offers BW value similar to that of the patch antenna without a resonator. In contrast, the hollow concave hemisphere exhibits a reduced BW, indicating limitations in its frequency range. When analyzing the radiation pattern, the concave hemisphere stands out with a notable improvement in terms of MLM, exceeding that of the patch antenna without a resonator. Moreover, it attains a reduction in HPBW and SLL, as listed in Table 5, contributing to enhanced directionality and overall radiation efficiency. Furthermore, the LPA half-cylinder increases the HPBW compared to the patch antenna without a resonator. Finally, the hemisphere geometry alters the MLD value compared to the patch antenna without a resonator.

Rectangular prism-based geometries exhibit reductions at the resonant frequency, as illustrated in Figure 8b, underscoring their potential for antenna size reduction. Despite this advantage, their performance at the resonant frequency yields an unacceptable $|S_{11}|$, Table 5. The radiation pattern analysis in Figure 10b shows contrasting behaviors. For instance, the rectangular prism geometry achieves a notable increase in the MLM value, maintaining a value higher than that of the patch antenna without a resonator, indicating its potential for improving radiation efficiency. In contrast, the hollow rectangular prism substantially decreases the MLM value. Furthermore, as summarized in Table 5, the rectangular prism achieves reductions in both HPBW and SLL and, consequently, enhances the directionality compared to the patch antenna without a resonator. Moreover, the hollow rectangular prism only yields a reduction in terms of HPBW and, unfortunately, with insignificant impact on SLL.

For the cone-based geometries, the analysis of $|S_{11}|$, as shown in Figure 8c and detailed in Table 5, reveals that the inverted cone and cone achieve acceptable values. Furthermore, in terms of BW, the inverted cone outperforms the cone; however, its BW remains lower than that of the patch antenna without a resonator, as listed in Table 5. Regarding the radiation pattern, depicted in Figure 10c and summarized in Table 5, the inverted cone exhibits the highest MLM value, followed by the cone, with both exceeding the performance of the patch antenna. The inverted cone also exhibits reductions in both HPBW and SLL compared to the patch antenna without a resonator, enhancing the directionality of the patch antenna. In contrast, the hollow inverted cone and cone geometries only achieve reductions in terms of HPBW.

Analyzing the half-cylinder-based geometries, it is clear that the LPA half-cylinder attains a significant reduction in the value of the resonant frequency, as shown in Figure 9a, highlighting its potential for minimizing patch antenna size. This is followed by the LPA hollow inverted half-cylinder and the WPA inverted and hollow inverted half-cylinders. As detailed in Table 5, the WPA hollow inverted half-cylinder achieves the highest BW value, in contrast to the LPA half-cylinder-based geometries. Observing the radiation pattern in Figure 11a and the values in Table 5, we conclude that the WPA inverted half-cylinder and half-cylinder geometries achieve MLM values higher than the patch antenna without a resonator. Concerning the HPBW parameter, the LPA half-cylinder offers better results than the patch antenna without a resonator, while the others yield lower ones. Taking a look at the SLL, the numerical results show that the LPA half-cylinder and the WPA inverted half-cylinder exhibit reductions compared to the patch antenna without a resonator, enhancing its directionality.

For the trapezoidal prism-based geometries, Figure 9b illustrates $|S_{11}|$. It can be seen that the LPA hollow inverted trapezoidal and trapezoidal prism geometries outperform the patch antenna without a resonator in terms of $|S_{11}|$. The WPA inverted trapezoidal

and trapezoidal prisms show potential for designing antennas with multiple resonant frequencies. Regarding BW, as listed in Table 5, the LPA trapezoidal prism achieves the highest value among these geometries, maintaining performance close to the patch antenna without a resonator. The radiation pattern plots, shown in Figure 11b and detailed in Table 5, reveals that the MLM values generally exceed the patch antenna without a resonator, except for the LPA trapezoidal prism. Furthermore, all the trapezoidal prism-based geometries exhibit reductions in terms of HPBW and improve the antenna directionality. In terms of SLL, most of the prism-based geometries show reductions, with the exceptions being the LPA trapezoidal prism and WPA hollow trapezoidal prism.

Overall, the analyses of the chosen geometries shapes for glycerin resonators show that the LPA hollow inverted trapezoidal and trapezoidal prism geometries exhibit the highest $|S_{11}|$ values. In terms of BW, the LPA trapezoidal prism achieves the widest BW, followed by the WPA hollow inverted half-cylinder and concave hemisphere. Moreover, several geometries show potential for antenna size reduction, with the cylindrical hemisphere performing best in this regard because it offers multiple resonant frequencies. In terms of MLM, the concave hemisphere and LPA inverted trapezoidal prism show significant improvements compared to the patch antenna without a resonator. Regarding the HPBW, the hemisphere exhibits the most substantial decrease, while the LPA half-cylinder shows an increase compared to the patch antenna without a resonator. Lastly, the rectangular prism offers the lowest SLL value.

4.3. Graphite Resonator

This subsection analyzes the numerical results when the patch antenna is combined with a graphite-made resonator when the chosen geometric shapes are considered. To support the analysis, $|S_{11}|$ for the cap-based, rectangular prism-based, cone-based, half-cylinder-based, and trapezoidal prism-based geometries are shown in Figure 12a, Figure 12b, Figure 12c, Figure 13a, and Figure 13b, respectively. Furthermore, the radiation patterns for the cap-based, rectangular prism-based, cone-based, half-cylinder-based, and trapezoidal prism-based geometries are illustrated in Figure 14a, Figure 14b, Figure 14c, Figure 15a, and Figure 15b, respectively. Moreover, Table 6 summarizes key parameter values obtained at the resonant frequency.

For the cap-based shape geometries, the plots of $|S_{11}|$ in Figure 13a show that both the concave hemisphere and hollow concave hemisphere exhibit similar performance, which is characterized by a slight downshift of the resonant frequency. In contrast, the cylindrical hemisphere shows a right resonant frequency shift. However, the hemisphere presents a significant reduction in the resonant frequency value and obtains an unacceptable $|S_{11}|$. Regarding BW, most of the evaluated geometries exhibit higher values than the patch antenna without a resonator, as summarized in Table 6. However, the cylindrical hemisphere stands out as the most prominent, achieving a BW value exceeding the patch antenna without a resonator. Considering the radiation pattern plots in Figure 14a and detailed in Table 6, we see that the concave and hollow concave hemispheres attain similar performance. Additionally, these two geometries achieve MLM values significantly higher compared to the patch antenna without a resonator, suggesting their potential for improving radiation efficiency. Regarding the HPBW, the concave and hollow concave hemispheres exhibit a reduction compared to the patch antenna without a resonator, signifying enhanced directionality. In contrast, the cylindrical hemisphere and hemisphere yield higher HPBW. Regarding SLL, only the concave and hollow concave hemispheres offer a reduction compared to the patch antenna without a resonator.

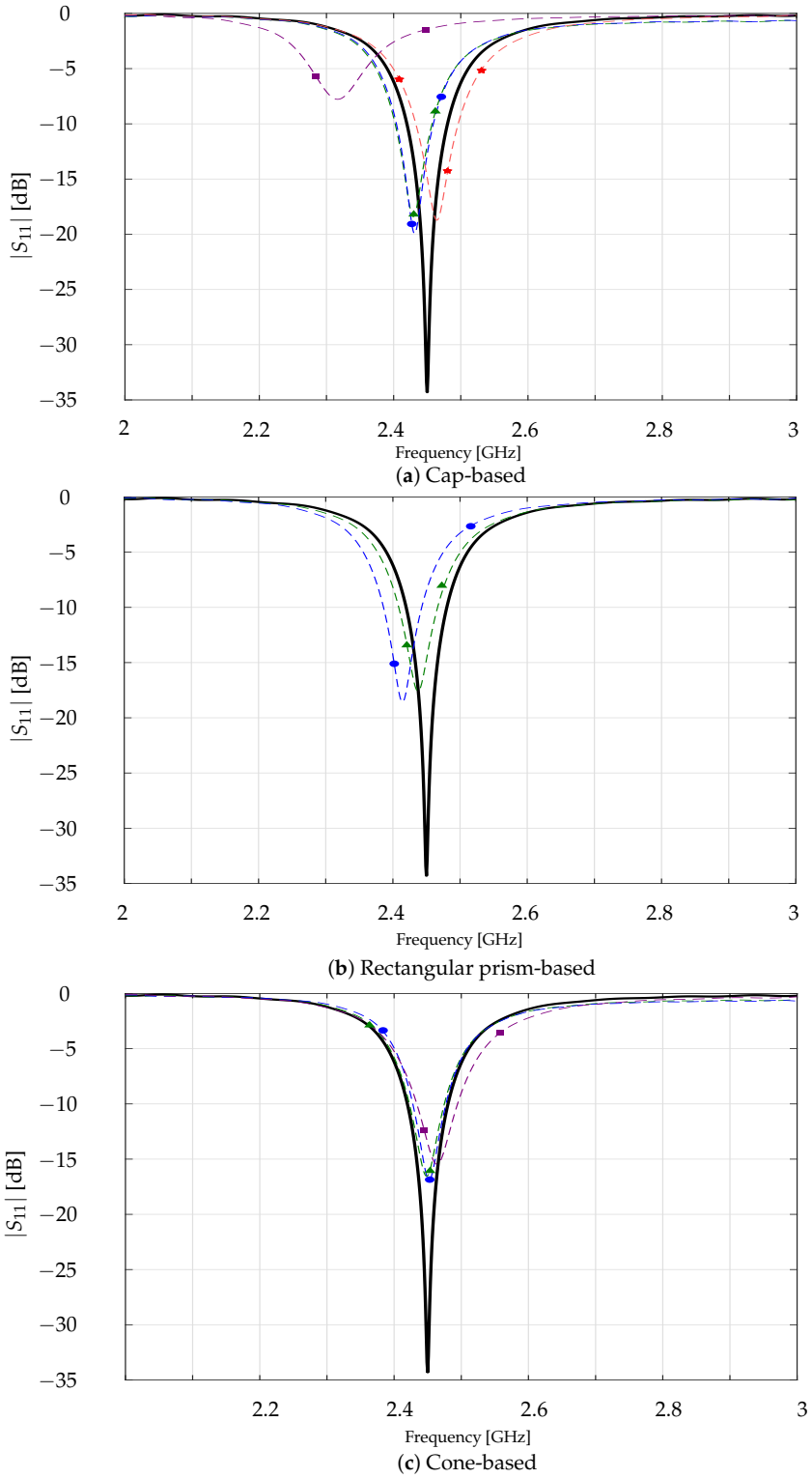


Figure 12. Patch antenna with a graphite-made resonator: magnitude of the scattering parameter ($|S_{11}|$). (**a**) cap-based; (**b**) rectangular prism-based; and (**c**) cone-based.

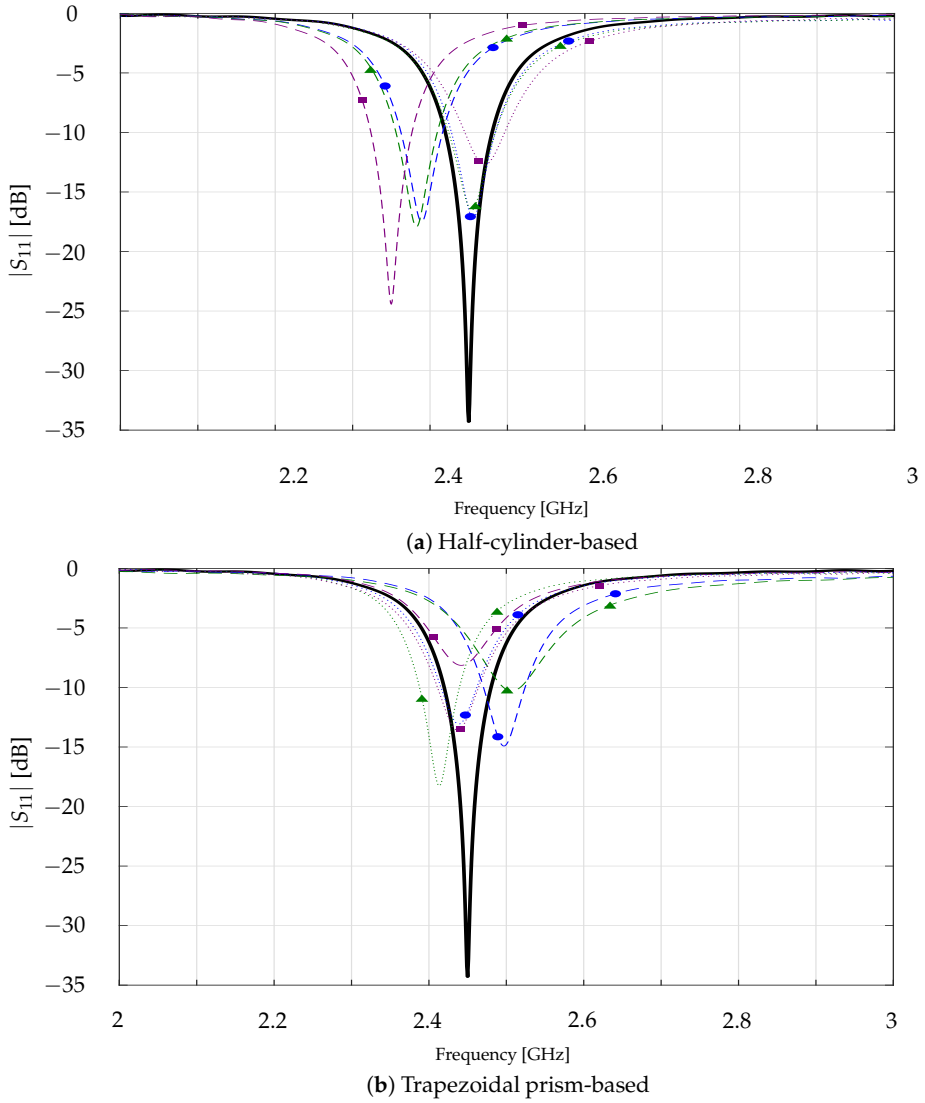
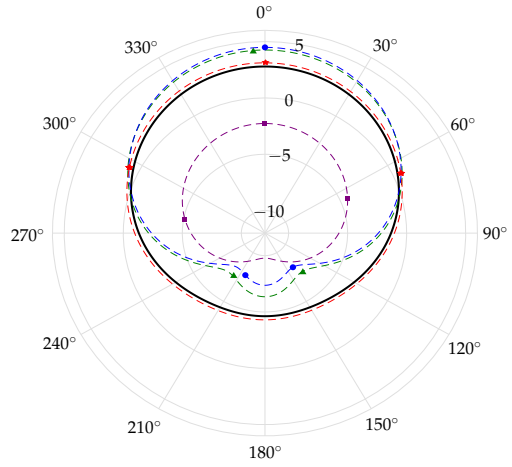
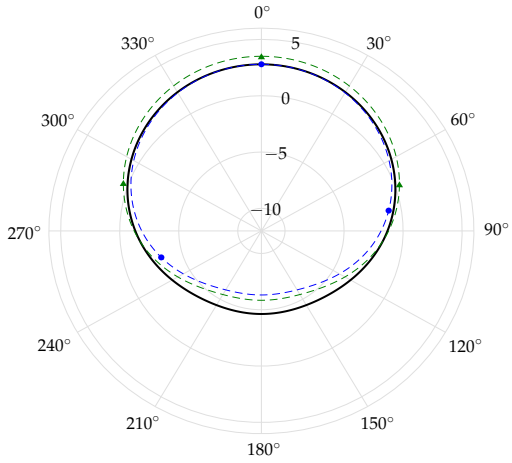


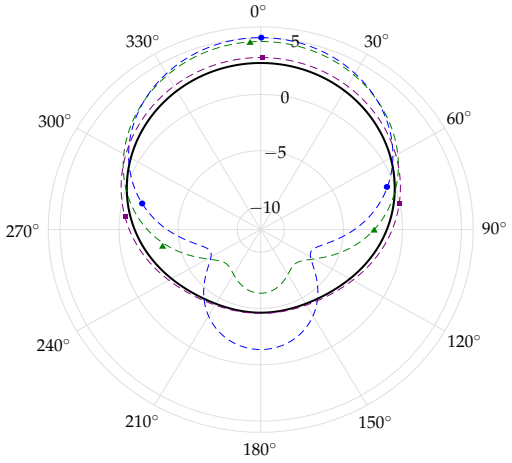
Figure 13. Patch antenna with a graphite-made resonator: magnitude of the scattering parameter ($|S_{11}|$). (**a**) half-cylinder-based; and (**b**) trapezoidal prism-based.



(**a**) Cap-based



(**b**) Rectangular prism-based



(**c**) Cone-based

Patch antenna
(**a**) Cylindrical hemisphere
Concave hemisphere
Hollow concave hemisphere
Hemisphere
(**b**) Rectangular prism
Hollow rectangular prism
(**c**) Inverted cone
Hollow inverted cone
Cone

Figure 14. Patch antenna with a graphite-made resonator: the radiation pattern plot of the 1D far-field realized gain ($\phi = 0$). (**a**) cap-based; (**b**) rectangular prism-based; and (**c**) cone-based.

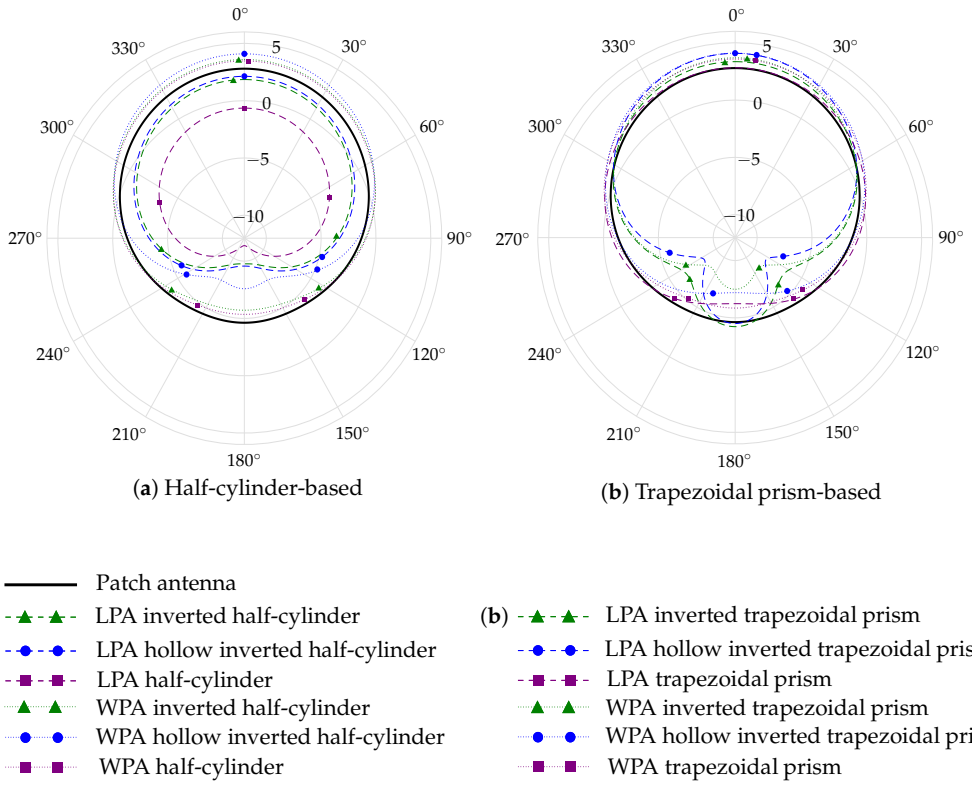


Figure 15. Patch antenna with a graphite-made resonator: the radiation pattern plot of the 1D far-field realized gain ($\phi = 0$). (**a**) half-cylinder-based; and (**b**) trapezoidal prism-based.

Table 6. Patch antenna with a graphite-made resonator: Key parameters values at the resonant frequency.

Geometry	$\lvert S_{11}\rvert$ (dB)	BW (MHz)	MLM (dBi)	HPBW (°)	SLL (dB)
Patch antenna	−34.30	60	2.79	148.2	w/o
Rectangular prism	−14.70	57	3.27	126.9	−11.1
Hollow rectangular prism	−8.46	42	2.79	139.1	w/o
Cylindrical hemisphere	−14.84	62	3.09	149.1	w/o
Concave hemisphere	−11.97	54	4.25	121	−10.6
Hollow concave hemisphere	−12.76	54	4.49	115.1	−11.9
Hemisphere	−1.44	w/o	−2.27	164.6	w/o
Inverted cone	−16.49	51	4.7	114	−11.1
Hollow inverted cone	−16.74	49	5.04	102.1	−6.4
Cone	−13.55	60	3.27	148.7	w/o
LPA Inverted half-cylinder	−4.19	9	1.84	129.8	w/o
LPA hollow inverted half-cylinder	−4.81	16	2.12	129.5	w/o
LPA half-cylinder	−2.32	w/o	−0.65	135.3	w/o
WPA inverted half-cylinder	−16.27	59	3.59	143.3	w/o
WPA hollow inverted half-cylinder	−16.48	56	4.08	129.6	−11.7
WPA half-cylinder	−10.76	50	3.47	146	w/o
LPA inverted trapezoidal prism	−5.76	3	3.35	128.2	−7.6
LPA hollow inverted trapezoidal prism	−6.45	29	4.08	114.6	−8.6
LPA trapezoidal prism	−7.97	w/o	2.82	164.3	w/o
WPA inverted trapezoidal prism	−7.68	39	3.69	120.4	−11.2
WPA hollow inverted trapezoidal prism	−12.07	45	4.09	127.8	w/o
WPA trapezoidal prism	−12.43	52	3.58	143.3	w/o

Analysis of the rectangular prism-based geometries reveals similar performances in terms of $\lvert S_{11}\rvert$, as illustrated in Figure 13b. The rectangular and hollow rectangular prisms show a slight shift in resonant frequency, with the hollow rectangular prism displaying

the most pronounced change. Moreover, the BW values listed in Table 6 are relatively broader for both geometries, with those associated with the rectangular prism being the closest to the patch antenna without a resonator. According to the radiation pattern plots, as depicted in Figure 14b, the rectangular prism offers an MLM that exceeds the patch antenna with a resonator. In contrast, the hollow rectangular prism shows an MLM similar to the patch antenna a with a resonator. Paying attention to the HPBW and SLL parameters, the rectangular prism shows the highest reduction compared to the patch antenna without a resonator, Table 6.

In relation to the cone-base shape geometries, similar $|S_{11}|$ values are obtained, as shown in Figure 13c. All geometries exhibit a broader BW except the cone, which attains a value similar to the patch antenna without a resonator. Concerning the radiation pattern, as depicted in Figure 14c, all the geometries exceed the MLM value of the patch antenna without a resonator. The hollow inverted cone and inverted cone exhibit similar performance in terms of MLM and achieve a relevant reduction in both HPBW and SLL, Table 6, and, consequently, they can be advanced to improve antenna directionality.

In regards to the half-cylinder geometries, $|S_{11}|$ in Figure 13a shows distinct performance trends based on the type of alignment. Geometries with the LPA alignment exhibit similar behavior to one another, as do those using the WPA alignment. Using LPA offers a downshift in the resonant frequency, suggesting their potential for reducing antenna size. In terms of BW, as listed in Table 6, geometries with WPA achieve the highest BW values compared to the patch antenna without a resonator. In contrast, geometries using LPA reduce the BW values. The radiation patterns in Figure 15a show geometries using WPA achieve MLM values higher than the patch antenna without a resonator. Conversely, geometries using LPA exhibit lower MLM values. Furthermore, among the evaluated geometries, the hollow half-cylinder achieves the highest MLM values when the alignments are considered. This are followed by the inverted half-cylinder geometries, with the half-cylinder geometries exhibiting the lowest MLM values. This trend highlights how relevant the type of alignment of geometries of the resonator over the patch antenna is in terms of radiation. When examining the SLL, only the WPA hollow inverted half-cylinder exhibits a change, showing a reduction in its SLL value. Consequently, it shows a unique behavior among the evaluated geometries, where the WPA hollow inverted half-cylinder enhances antenna directionality because SLL is reduced. Regarding the HPBW, all half-cylinder geometries attain lower values compared to the patch antenna without a resonator.

Concerning the trapezoidal prism-based geometries, $|S_{11}|$ in Figure 13b shows a slight shift in the resonant frequency. This shift is more pronounced for the LPA inverted trapezoidal prism and hollow inverted trapezoidal prism, as well as for the WPA inverted trapezoidal prism. Moreover, the BW is the largest for the WPA trapezoidal prism. The radiation pattern plots in Figure 15b show all trapezoidal prism-based geometries achieve higher MLM values compared to the patch antenna without a resonator, indicating their usefulness for enhancing radiation performance. According to Table 6, the LPA and WPA hollow inverted trapezoidal prisms exhibit the highest MLM values. In terms of HPBW, Table 6, most trapezoidal prism-based geometries show a reduction compared to the patch antenna without a resonator, except the LPA trapezoidal prism. Regarding the SLL, reductions are observed for the LPA inverted trapezoidal and hollow inverted trapezoidal prisms, improving antenna performance. Similar enhancements are also noted for the WPA inverted trapezoidal prism, Table 6. Lastly, these geometries show a reduction in their SLL values, indicating their usefulness for improving antenna directionality.

Overall, analyzing various geometry shapes for graphite resonators, several trends emerge across the different geometries. Most are characterized by a slight shift in resonant frequency, with the most significant changes observed in the half-cylinder-based geometries,

mainly aligned in the LPA half-cylinder-based geometries, and for the hemisphere within the cap-based geometries. Regarding BW, the highlight is the cylindrical hemisphere, which exhibits a BW value higher than the patch antenna without a resonator. This is followed by the cone, which obtains BW value similar to the patch antenna without a resonator. Regarding the MLM value, the greatest improvement is observed in the hollow inverted cone, which outperforms the other geometries. The hollow inverted cone also shows the highest reduction in HPBW, indicating a more focused radiation pattern and enhanced directionality than the patch antenna without a resonator. Among the geometry shapes that present changes in SLL, the hollow concave hemisphere achieves the greatest reduction in this value and enhances its directionality.

4.4. General Comments

The numerical results analyzed in previous sections reveal that performance can significantly vary with the choice of material and geometry of the resonator when the performance evaluation parameters (e.g., $|S_{11}|$, BW, and MLM) are considered. Specifically, the graphite resonators exhibit the highest number of geometric shapes with better MLM compared to the patch antenna without a resonator, followed by DW resonators and the glycerin resonators, respectively. Among the combination of material and geometries with MLM exceeding that of the patch antenna without a resonator, the combinations using DW attain the majority of acceptable $|S_{11}|$ values, followed by those using graphite, and, finally, those using glycerin. Moreover, when combined with the appropriate geometry, each resonator material enhances the radiation pattern. Several of the evaluated resonators achieved MLM values exceeding 5 dBi, indicating improved radiation efficiency.

Moreover, certain resonators show reductions in HPBW and SLL, improving antenna directionality. For instance, the inverted cone resonator with DW material achieves the highest improvements in terms of MLM and interesting reductions in HPBW and SLL, compared to the patch antenna without a resonator. Furthermore, this resonator maintains an acceptable $|S_{11}|$ at the resonant frequency of 2.45 GHz. Similarly, the DW material in the LPA hollow inverted prism and inverted prism geometric shapes also achieves MLM values greater than 5 dBi, provide significant reductions in terms of HPBW and SLL, resulting in improved directionality while maintaining acceptable $|S_{11}|$.

Resonators based on glycerin material also achieve MLM values exceeding 5 dBi, indicating enhanced radiation efficiency. Among these, the concave hemisphere exhibits the highest MLM, followed by the LPA inverted trapezoidal prism. Furthermore, use of this material improves antenna directionality due to the attained reductions in HPBW and SLL. Moreover, these resonators maintain acceptable $|S_{11}|$, with the LPA inverted trapezoidal prism showing superior performance. Using graphite results in resonators that are slightly outperformed by DW and glycerin resonators. When the hollow inverted cone is considered, its use achieves an MLM greater than 5 dBi. This resonator also achieves reductions in HPBW and SLL while maintaining an acceptable $|S_{11}|$. As a result of these characteristics, the antenna performance is enhanced.

Using resonators is an effective approach to enhancing some performance parameters of a patch antenna; however, it can also degrade certain others. For instance, a hollow rectangular prism can influence the performance of a patch antenna differently depending on the material used, and when made of DW, it improves the SLL but negatively affects other parameters. Conversely, when filled with glycerin, it enhances only the HPBW, whereas, with graphite, it preserves the SLL and MLM while also improving the HPBW. Similarly, depending on the material, the WPA hollow inverted half-cylinder resonator exhibits different effects. When constructed from DW or glycerin, it improves only the HPBW. However, when made from graphite, it enhances the MLM, HPBW, and SLL.

Furthermore, the hollow rectangular prism exhibited degraded impedance matching, while half-cylinder-based geometries led to shifts in the resonant frequency without significant improvements in BW or radiation efficiency.

In Tables 7–9, we compare the material and geometric combinations analyzed in our study with those explored in previous works. It should be noted that the previous research cited in Table 7 examined cylinder shapes in a different orientation than in our study. Furthermore, some geometries investigated in our work have not been previously explored. While our results align with those reported in the literature, our approach provides a broader perspective. By analyzing multiple geometries composed of the same material and variations involving different materials, we extend the scope of analysis. This comprehensive investigation offers deeper insights into the interaction between geometry and material selection, further enhancing existing findings.

Overall, the results emphasize the importance of selecting the appropriate material and geometry to improve antenna performance regarding the radiation pattern while maintaining the magnitude of $|S_{11}|$ below -10 dB. A comparison of the numerical results for highlighting the combination of material and geometries offering the best MLM is shown in Figure 16.

Table 7. Comparison of the DW resonator with different geometric shapes analyzed in our work and in previous studies.

Material	Geometry Shapes	Our Work	Previous Work
DW	Rectangular prism	✓	[9,40]
	Hollow rectangular prism	✓	w/o
	Cylindrical hemisphere	✓	w/o
	Concave hemisphere	✓	w/o
	Hollow concave hemisphere	✓	w/o
	Hemisphere	✓	[41,42]
	Inverted cone	✓	w/o
	Hollow inverted cone	✓	w/o
	Cone	✓	w/o
	LPA Inverted half-cylinder	✓	[43]
	LPA hollow inverted half-cylinder	✓	[43]
	LPA half-cylinder	✓	[43]
	WPA inverted half-cylinder	✓	[43]
	WPA hollow inverted half-cylinder	✓	[43]
	WPA half-cylinder	✓	[43]
	LPA inverted trapezoidal prism	✓	w/o
	LPA hollow inverted trapezoidal prism	✓	w/o
	LPA trapezoidal prism	✓	w/o
	WPA inverted trapezoidal prism	✓	w/o
	WPA hollow inverted trapezoidal prism	✓	w/o
	WPA trapezoidal prism	✓	w/o

Table 8. Comparison of the glycerin resonator with different geometric shapes analyzed in our work and in previous studies.

Material	Geometry Shapes	Our Work	Previous Work
Glycerin	Rectangular prism	✓	w/o
	Hollow rectangular prism	✓	w/o
	Cylindrical hemisphere	✓	[44,45]
	Concave hemisphere	✓	w/o
	Hollow concave hemisphere	✓	w/o
	Hemisphere	✓	w/o
	Inverted cone	✓	w/o
	Hollow inverted cone	✓	w/o
	Cone	✓	[46]

Table 8. *Cont.*

Material	Geometry Shapes	Our Work	Previous Work
Glycerin	LPA Inverted half-cylinder	✓	w/o
	LPA hollow inverted half-cylinder	✓	w/o
	LPA half-cylinder	✓	w/o
	WPA inverted half-cylinder	✓	w/o
	WPA hollow inverted half-cylinder	✓	w/o
	WPA half-cylinder	✓	[47–49]
	LPA inverted trapezoidal prism	✓	w/o
	LPA hollow inverted trapezoidal prism	✓	w/o
	LPA trapezoidal prism	✓	w/o
	WPA inverted trapezoidal prism	✓	w/o
	WPA hollow inverted trapezoidal prism	✓	w/o
	WPA trapezoidal prism	✓	w/o

Table 9. Comparison of the graphite resonator with different geometric shapes analyzed in our work and in previous studies.

Material	Geometry Shapes	Our Work	Previous Work
Graphite	Rectangular prism	✓	[6,50]
	Hollow rectangular prism	✓	w/o
	Cylindrical hemisphere	✓	w/o
	Concave hemisphere	✓	w/o
	Hollow concave hemisphere	✓	w/o
	Hemisphere	✓	w/o
	Inverted cone	✓	w/o
	Hollow inverted cone	✓	w/o
	Cone	✓	w/o
	LPA Inverted half-cylinder	✓	w/o
	LPA hollow inverted half-cylinder	✓	w/o
	LPA half-cylinder	✓	w/o
	WPA inverted half-cylinder	✓	w/o
	WPA hollow inverted half-cylinder	✓	w/o
	WPA half-cylinder	✓	w/o
	LPA inverted trapezoidal prism	✓	w/o
	LPA hollow inverted trapezoidal prism	✓	w/o
	LPA trapezoidal prism	✓	w/o
	WPA inverted trapezoidal prism	✓	w/o
	WPA hollow inverted trapezoidal prism	✓	w/o
	WPA trapezoidal prism	✓	w/o

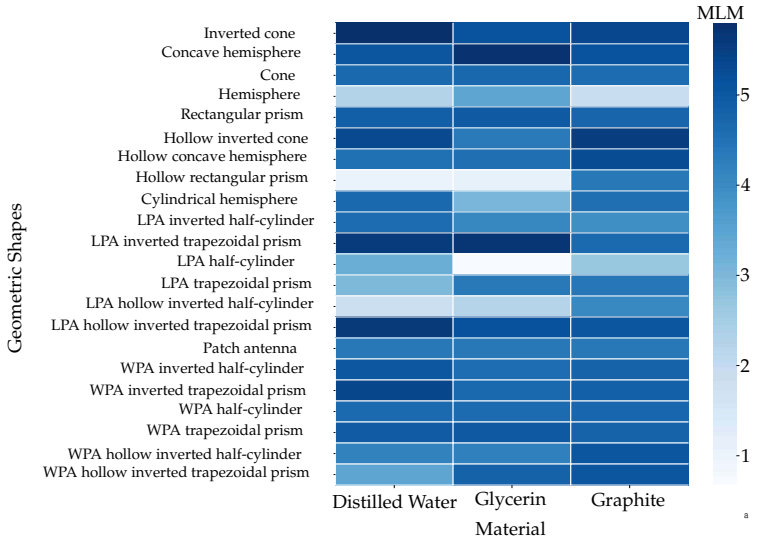


Figure 16. Comparison in terms of MLM between the combinations of materials and geometries.

5. Conclusions

This paper provided a comprehensive study on patch antennas embedded in dielectric and conductive material-based resonators, examining their effects on key performance parameters such as impedance matching, bandwidth, radiation efficiency, and gain. The study systematically investigated fifteen distinct geometric resonator shapes composed of distilled water, glycerin, and graphite, providing valuable insights into their influence on antenna behavior.

The numerical results highlighted that specific resonator geometries, particularly combined with a high dielectric constant material, effectively enhance bandwidth, improve impedance matching, and increase radiation efficiency. We also observed that certain geometries allow multi-band operation due to multiple impedance matching points. Conversely, the study also identified cases where the inclusion of a resonator does not yield a substantial performance enhancement. In a few cases, it even degrades the performance of a patch antenna. Specifically, some configurations exhibited degraded impedance matching, while others led to shifts in the resonant frequency without significant bandwidth or radiation efficiency improvements. These findings emphasize the importance of careful material and geometric selections for achieving meaningful performance gains.

Overall, this paper contributes to advancing patch antenna design by offering insights and guidance for selecting one of the fifteen geometric shapes and one of the three materials (distilled water, glycerin, and graphite) for embedding a patch antenna into a resonator. The discussions are particularly relevant in scenarios requiring compact designs, enhanced efficiency, or multi-band operation. Future work may focus on other materials, an array of patch antennas, experimental validation, and further resonator–container fabrication combinations to address practical implementation challenges.

Author Contributions: Conceptualization, C.M.S.F.; Data curation, C.M.S.F. and C.M.M.A.; Formal analysis, C.M.S.F., L.G.S.C., B.R.D. and M.V.R.; Investigation, C.M.S.F. and C.M.M.A.; Methodology, C.M.S.F., C.M.M.A., L.G.S.C., B.R.D. and M.V.R.; Supervision, M.V.R.; Validation, B.R.D., M.A.O.S., G.L.R. and M.V.R.; Visualization, C.M.S.F., C.M.M.A. and L.G.S.C.; Writing—original draft, C.M.S.F., C.M.M.A. and L.G.S.C.; Writing—review and editing, B.R.D., M.A.O.S., G.L.R. and M.V.R. All authors have read and agreed to the published version of the manuscript.

Funding: This research was supported in part by Coordenação de Aperfeiçoamento de Pessoal de Nível Superior (CAPES) under Grant 001; Conselho Nacional de Desenvolvimento Científico e Tecnológico (CNPq) under grants 404068/2020-0, 314741/2020-8, and 445958/2024-3; Fundação de Amparo à Pesquisa do Estado de Minas Gerais (FAPEMIG) under grants APQ-03609-17 and APQ-04623-22, and Instituto Nacional de Energia Elétrica (INERGE).

Institutional Review Board Statement: Not applicable.

Informed Consent Statement: Not applicable.

Data Availability Statement: All data supporting the results reported in this study are provided in the Appendix of this manuscript.

Conflicts of Interest: The authors declare no conflicts of interest. The funders had no role in the design of the study; in the collection, analyses, or interpretation of data; in the writing of the manuscript, or in the decision to publish the results.

Abbreviations

The following abbreviations are used in this manuscript:

BW	bandwidth
CST	Computer Simulation Technology
DW	distilled water
FD	frequency-domain
FR-4	flame retardant-4
HPBW	half-power beamwidth
LPA	length of the patch antenna
MLD	main lobe direction
MLM	main lobe magnitude
PML	perfectly matched Layers
RF	radio frequency
SLL	side lobe level
TD	time-domain
TE	transverse electric
TM	transverse magnetic
WG	whispering gallery
WPA	width of the patch antenna

Appendix A. Information on Geometry Dimensions

This appendix provides the resonator dimensions for the geometries depicted in Figure 2. For geometries using WPA, the variables are marked with a prime symbol′, while no prime symbol is used for geometries with LPA.

For performing the numerical simulations with CST software, the parameters of each geometry varied in the interval given by $[L_{\text{bound}}, U_{\text{bound}}]$ when the values of the parameters are taken using a resolution equal to Δ. Table A1 lists for each geometry, the values of L_{bound}, U_{bound}, and Δ.

Moreover, Tables A2–A4 list the values of the dimensions obtained in the numerical simulations for geometries combined to DW, glycerin, and graphite materials when the highest values of MLM is considered.

Table A1. Dimensions (in mm) and corresponding ranges for various geometric shapes.

Geometry	Parameter	L_{bound}	U_{bound}	Δ
Retangular prism	h_{rp}	1	20	0.1
	L_{rp}	15	35	1
Hollow rectangular prism	h_{hrp}	1	20	0.1
Cylindrical hemisphere	r_{hy}	1	30	0.1
Concave hemisphere	r_{sp}	16	30	0.1
Hollow concave hemisphere	r_{sph}	16	30	0.1
Hemisphere	r_{spc}	16	30	0.01
Inverted cone	h_{conc}	1	30	0.05
	r_{t}	7.1	40	0.05
Hollow inverted cone	h_{ch}	1	30	0.05
	r_{th}	7.1	30	0.1
Cone	h_{conv}	1	30	0.05
	r_{bc}	7.1	30	0.1
LPA inverted half-cylinder	r_{cy}	1	20	0.1
LPA hollow inverted half-cylinder	r_{cyh}	1	20	0.1
LPA half-cylinder	r_{cyc}	1	20	0.1

Table A1. *Cont.*

Geometry	Parameter	L_{bound}	U_{bound}	Δ
WPA inverted half-cylinder	r'_{cy}	3	20	0.1
WPA hollow inverted half-cylinder	r'_{cyh}	1	20	0.1
WPA half-cylinder	r'_{cyc}	3	20	0.1
LPA inverted trapezoidal prism	h_{p}	1	30	0.1
	L_{bs}	15	35	0.1
LPA hollow inverted trapezoidal prism	h_{ph}	10	30	0.1
	L_{bsh}	15	35	1
LPA trapezoidal prism	h_{pc}	1	30	1
	L_{bsc}	15	35	1
WPA inverted trapezoidal prism	h'_{p}	3	30	1
	W'_{bs}	30	33	1
WPA hollow inverted trapezoidal prism	h'_{ph}	3	30	1
	W'_{bsh}	30	33	1
WPA trapezoidal prism	h'_{pc}	10	30	1
	W'_{bsc}	3	10	2
	L'_{bsc}	3	10	1

Table A2. The DW-made resonator: The dimensions (in mm) offering the best MLM in the numerical simulations.

Geometry	Parameter	Value	Geometry	Parameter	Value
Rectangular prism	h_{rp}	7.00	LPA half-cylinder	r_{cyc}	8.60
	L_{rp}	29.00		L_{cyc}	30.00
	W_{rp}	15.00		W_{cyc}	19.86
Hollow rectangular prism	h_{hrp}	17.80	WPA inverted half-cylinder	r'_{cy}	19.00
	L_{hrp}	32.00		L'_{cyl}	28.80
	W_{hrp}	18.00		W'_{cyl}	18.00
Cylindrical hemisphere	h_{hy}	1.44	WPA hollow inverted half-cylinder	r'_{cyh}	3.00
	r_{hy}	8.40		L'_{cyh}	28.77
				W'_{cyh}	15.00
				t'_{cyh}	1.00
Concave hemisphere	r_{sp}	22.70	WPA half-cylinder	r'_{cyc}	6.90
				L'_{cyc}	28.80
				W'_{cyc}	18.00
Hollow concave hemisphere	r_{sph}	16.00	LPA inverted trapezoidal prism	h_{p}	26.50
				L_{bs}	28.20
				W_{bs}	28.28
				L_{bip}	14.00
				W_{bip}	15.21
Hemisphere	r_{spc}	22.97	LPA inverted hollow trapezoidal prism	h_{ph}	21.30
				L_{bsh}	28.00
				W_{bsh}	28.28
				L_{bih}	14.00
				W_{bih}	15.21
				t_{ph}	4.95
Inverted cone	h_{conc}	27.25	LPA trapezoidal prism	h_{pc}	25.00
	r_{b}	7.75		L_{bsc}	35.00
	r_{t}	14.25		W_{bsc}	15.21
				L_{bipc}	28.00
				W_{bipc}	28.28

Table A2. *Cont.*

Geometry	Parameter	Value	Geometry	Parameter	Value
Hollow inverted cone	h_{ch}	19.00	WPA inverted trapezoidal prism	h'_{p}	21.00
	r_{bh}	7.00		L'_{bs}	28.83
	r_{th}	14.00		W'_{bs}	33.00
	t_{ch}	6.02		L'_{bip}	14.00
				W'_{bip}	15.21
Cone	h_{conv}	10.15	WPA hollow inverted trapezoidal prism	h'_{ph}	30.00
	r_{bc}	8.60		L'_{bsh}	30.00
	r_{tc}	14.00		W'_{bsh}	31.00
				L'_{bih}	28.83
				W'_{bih}	15.00
				t'_{ph}	4.95
LPA inverted half-cylinder	r_{cy}	15.90	WPA trapezoidal prism	h'_{pc}	14.00
	L_{cyl}	30.00		L'_{bsc}	10.00
	W_{cyl}	19.97		W'_{bsc}	3.00
				L'_{bipc}	28.83
				W'_{bipc}	15.00
LPA hollow inverted half-cylinder	r_{cyh}	2.10			
	L_{cyh}	30.00			
	W_{cyh}	19.96			
	t_{cyh}	1.00			

Table A3. The glycerin-made resonator: The dimensions (in mm) offering the best MLM in the numerical simulations.

Geometry	Parameter	Value	Geometry	Parameter	Value
Rectangular prism	h_{rp}	7.00	LPA half-cylinder	r_{cyc}	8.60
	L_{rp}	29.00		L_{cyc}	30.00
	W_{rp}	15.00		W_{cyc}	19.86
Hollow rectangular prism	h_{hrp}	17.80	WPA inverted half-cylinder	r'_{cy}	19.00
	L_{hrp}	32.00		L'_{cyl}	28.80
	W_{hrp}	18.00		W'_{cyl}	18.00
Cylindrical hemisphere	h_{hy}	1.44	WPA hollow inverted half-cylinder	r'_{cyh}	3.00
	r_{hy}	8.40		L'_{cyh}	28.77
				W'_{cyh}	15.00
				t'_{cyh}	1.00
Concave hemisphere	r_{sp}	22.70	WPA half-cylinder	r'_{cyc}	6.90
				L'_{cyc}	28.80
				W'_{cyc}	18.00
Hollow concave hemisphere	r_{sph}	16.00	LPA inverted trapezoidal prism	h_{p}	26.50
				L_{bs}	28.20
				W_{bs}	28.28
				L_{bip}	14.00
				W_{bip}	15.21
Hemisphere	r_{spc}	22.97	LPA inverted hollow trapezoidal prism	h_{ph}	21.30
				L_{bsh}	28.00
				W_{bsh}	28.28
				L_{bih}	14.00
				W_{bih}	15.21
				t_{ph}	4.95

Table A3. *Cont.*

Geometry	Parameter	Value	Geometry	Parameter	Value
Inverted cone	h_{conc}	27.25	LPA trapezoidal prism	h_{pc}	25.00
	r_b	7.75		L_{bsc}	35.00
	r_t	14.25		W_{bsc}	15.21
				L_{bipc}	28.00
				W_{bipc}	28.28
Hollow inverted cone	h_{ch}	19.00	WPA inverted trapezoidal prism	h'_p	21.00
	r_{bh}	7.00		L'_{bs}	28.83
	r_{th}	14.00		W'_{bs}	33.00
	t_{ch}	6.02		L'_{bip}	14.00
				W'_{bip}	15.21
Cone	h_{conv}	10.15	WPA hollow inverted trapezoidal prism	h'_{ph}	30.00
	r_{bc}	8.60		L'_{bsh}	30.00
	r_{tc}	14.00		W'_{bsh}	31.00
				L'_{bih}	28.83
				W'_{bih}	15.00
				t'_{ph}	4.95
LPA inverted half-cylinder	r_{cy}	15.90	WPA trapezoidal prism	h'_{pc}	14.00
	L_{cyl}	30.00		L'_{bsc}	10.00
	W_{cyl}	19.97		W'_{bsc}	3.00
				L'_{bipc}	28.83
				W'_{bipc}	15.00
LPA hollow inverted half-cylinder	r_{cyh}	2.10			
	L_{cyh}	30.00			
	W_{cyh}	19.96			
	t_{cyh}	1.00			

Table A4. The graphite-made resonator: The dimensions (in mm) offering the best MLM in the numerical simulations.

Geometry	Parameter	Value	Geometry	Parameter	Value
Rectangular prism	h_{rp}	20.00	LPA half-cylinder	r_{cyc}	10.00
	L_{rp}	29.00		L_{cyc}	30.00
	W_{rp}	15.00		W_{cyc}	14.98
Hollow rectangular prism	h_{hrp}	4.00	WPA inverted half-cylinder	r'_{cy}	20.00
	L_{hrp}	29.00		L'_{cyl}	19.97
	W_{hrp}	15.00		W'_{cyl}	18.00
Cylindrical hemisphere	h_{hy}	2.00	WPA hollow inverted half-cylinder	r'_{cyh}	20.00
	r_{hy}	6.60		L'_{cyh}	28.80
				W'_{cyh}	18.00
				t'_{cyh}	1.00
Concave hemisphere	r_{sp}	18.50	WPA half-cylinder	r'_{cyc}	20.00
				L'_{cyc}	18.00
				W'_{cyc}	14.97
Hollow concave hemisphere	r_{sph}	18.60	LPA inverted trapezoidal prism	h_p	30.00
				L_{bs}	28.00
				W_{bs}	28.28
				L_{bip}	14.00
				W_{bip}	15.21

Table A4. *Cont.*

Geometry	Parameter	Value	Geometry	Parameter	Value
Hemisphere	r_{spc}	16.00	LPA inverted hollow trapezoidal prism	h_{ph}	21.50
				L_{bsh}	35.00
				W_{bsh}	28.28
				L_{bih}	14.00
				W_{bih}	15.21
				t_{ph}	5.04
Inverted cone	h_{conc}	15.00	LPA trapezoidal prism	h_{pc}	27.00
	r_b	7.90		L_{bsc}	28.00
	r_t	20.90		W_{bsc}	15.21
				L_{bipc}	14.00
				W_{bipc}	28.28
Hollow inverted cone	h_{ch}	20.00	WPA inverted trapezoidal prism	h'_p	17.00
	r_{bh}	5.50		L'_{bs}	30.00
	r_{th}	20.10		W'_{bs}	30.00
	t_{ch}	12.27		L'_{bip}	28.83
				W'_{bip}	15.21
Cone	h_{conv}	15.00	WPA hollow inverted trapezoidal prism	h'_{ph}	10.00
	r_{bc}	7.10		L'_{bsh}	28.00
	r_{tc}	7.00		W'_{bsh}	33.00
				L'_{bih}	28.83
				W'_{bih}	15.00
				t'_{ph}	4.95
LPA inverted half-cylinder	r_{cy}	9.50	WPA trapezoidal prism	h'_{pc}	22.00
	L_{cyl}	30.00		L'_{bsc}	10.00
	W_{cyl}	19.95		W'_{bsc}	9.00
				L'_{bipc}	28.83
				W'_{bipc}	15.00
LPA hollow inverted half-cylinder	r_{cyh}	9.00			
	L_{cyh}	30.00			
	W_{cyh}	19.88			
	t_{cyh}	1.00			

References

1. Sarin, V.P.; Nassar, N.; Deepu, V.; Aanandan, C.K.; Mohanan, P.; Vasudevan, K. Wideband Printed Microstrip Antenna for Wireless Communications. *IEEE Antennas Wirel. Propag. Lett.* **2009**, *8*, 779–781. [CrossRef]
2. Ye, S.; Geng, J.; Liang, X.; Guo, Y.J.; Jin, R. A Compact Dual-Band Orthogonal Circularly Polarized Antenna Array with Disparate Elements. *IEEE Trans. Antennas Propag.* **2015**, *63*, 1359–1364. [CrossRef]
3. Huang, Y.; Xing, L.; Song, C.; Wang, S.; Elhouni, F. Liquid Antennas: Past, Present and Future. *IEEE Open J. Antennas Propag.* **2021**, *2*, 473–487. [CrossRef]
4. Balanis, C.A. *Antenna Theory, Analysis, and Design*, 4th ed.; John Wiley & Sons: Hoboken , NJ, USA, 2016.
5. Dash, S.K.K.; Khan, T.; De, A. Dielectric resonator antennas: An application oriented survey. *Int. J. RF Microw. Comput.-Aided Eng.* **2017**, *27*, e21069. [CrossRef]
6. Aldrigo, M.; Dragoman, M.; Iordanescu, S.; Avram, A.; Simionescu, O.G.; Parvulescu, C.; Ghannudi, H.E.; Montori, S.; Nicchi, L.; Xavier, S.; et al. Tunable 24-GHz Antenna Arrays Based on Nanocrystalline Graphite. *IEEE Access* **2021**, *9*, 122443–122456. [CrossRef]
7. Paracha, K.N.; Butt, A.D.; Alghamdi, A.S.; Babale, S.A.; Soh, P.J. Liquid Metal Antennas: Materials, Fabrication and Applications. *Sensors* **2020**, *20*, 177. [CrossRef]
8. Wang, C.; Yeo, J.C.; Chu, H.; Lim, C.T.; Guo, Y.X. Design of a Reconfigurable Patch Antenna Using the Movement of Liquid Metal. *IEEE Antennas Wirel. Propag. Lett.* **2018**, *17*, 974–977. [CrossRef]
9. Li, Y.; Luk, K.M. A Water Dense Dielectric Patch Antenna. *IEEE Access* **2015**, *3*, 274–280. [CrossRef]
10. Mukherjee, B.; Patel, P.; Mukherjee, J. A review of the recent advances in dielectric resonator antennas. *J. Electromagn. Waves Appl.* **2020**, *34*, 1095–1158. [CrossRef]

11. Lu, D.; Zhang, C.; Wang, Z.; Li, R.Z.; Yan, J.; Yu, Y. Design of Multibeam Conformal Antenna Based on Liquid Metal. *IEEE Antennas Wirel. Propag. Lett.* **2024**, *23*, 960–964. [CrossRef]
12. Malfajani, R.S.; Niknam, H.; Bodkhe, S.; Therriault, D.; Laurin, J.J.; Sharawi, M.S. A 3D-Printed Encapsulated Dual Wide-Band Dielectric Resonator Antenna With Beam Switching Capability. *IEEE Open J. Antennas Propag.* **2023**, *4*, 492–505. [CrossRef]
13. Halimi, M.A.; Khan, T.; Surender, D.; Nasimuddin, N.; Rengarajan, S.R. Dielectric Resonator Antennas for RF Energy-Harvesting/Wireless Power Transmission Applications: A state-of-the-art review. *IEEE Antennas Propag. Mag.* **2024**, *66*, 34–45. [CrossRef]
14. Salimitorkamani, M.; Mehranpour, M.; Odabasi, H. A Miniaturized Wideband Sinuous Antenna for Microwave Brain Imaging Systems. *IEEE Trans. Antennas Propag.* **2024**, *72*, 2228–2240. [CrossRef]
15. Varshney, G. Wideband THz Absorber: By Merging the Resonance of Dielectric Cavity and Graphite Disk Resonator. *IEEE Sens. J.* **2021**, *21*, 1635–1643. [CrossRef]
16. Su, Z.L.; Leung, K.W.; Lu, K. Gain Enhancement of Low-Profile Dielectric Resonator Antenna With a Loading Metal. *IEEE Antennas Wirel. Propag. Lett.* **2024**, *23*, 2718–2722. [CrossRef]
17. Niamien, C.; Collardey, S.; Sharaiha, A.; Mahdjoubi, K. Compact expressions for efficiency and bandwidth of patch antennas over lossy magneto-dielectric materials. *IEEE Antennas Wirel. Propag. Lett.* **2011**, *10*, 63–66. [CrossRef]
18. Keyrouz, S.; Caratelli, D. Dielectric Resonator Antennas: Basic Concepts, Design Guidelines, and Recent Developments at Millimeter-Wave Frequencies. *Int. J. Antennas Propag.* **2016**, *2016*, 6075680. [CrossRef]
19. Pozar, D.M. *Microwave Engineering*, 4th ed.; John Wiley & Sons, Inc.: Hoboken, NJ, USA, 2011.
20. Khan, A.; Nema, R. Analysis of Five Different Dielectric Substrates on Microstrip Patch Antenna. *Int. J. Comput. Appl.* **2012**, *55*, 40–47. [CrossRef]
21. Rodríguez, B.; Barboni, L.; Gómez, J.; Contreras, A. Size Reduction, Multiband and Beamforming Features by Embedding Antennas in Distilled Water. *Wirel. Pers. Commun.* **2023** , *129*, 881–889. [CrossRef]
22. Dash, U.A.; Sahu, S. UWB Dual-Band Notched Conical Dielectric Resonator Antenna with Improved Gain. *IETE J. Res.* **2020**, *66*, 643–653. [CrossRef]
23. Sun, J.; Luk, K. A Compact-Size Wideband Optically-Transparent Water Patch Antenna Incorporating an Annular Water Ring. *IEEE Access* **2019**, *7*, 122964–122971. [CrossRef]
24. Sun, J.; Luk, K.M. A Fully Transparent Wideband Water Patch Antenna With L-Shaped Feed. *IEEE Open J. Antennas Propag.* **2021**, *2*, 968–975. [CrossRef]
25. Wang, M.; Chu, Q. High-Efficiency and Wideband Coaxial Dual-Tube Hybrid Monopole Water Antenna. *IEEE Antennas Wirel. Propag. Lett.* **2018**, *17*, 799–802. [CrossRef]
26. Song, C.; Bennett, E.L.; Xiao, J.; Alieldin, A.; Luk, K.M.; Huang, Y. Metasurfaced, Broadband, and Circularly Polarized Liquid Antennas Using a Simple Structure. *IEEE Trans. Antennas Propag.* **2019**, *67*, 4907–4913. [CrossRef]
27. Liu, S.B.; Zhang, F.S.; Zhang, Y.X. Dual-band circular-polarization reconfigurable liquid dielectric resonator antenna. *Int. J. RF Microw. Comput.-Aided Eng.* **2019**, *29*, e21613. [CrossRef]
28. Gaya, A.; Jamaluddin, M.H.; Alali, B.; Althuwayb, A.A. A novel wide dual band circularly polarized dielectric resonator antenna for milli meter wave 5G applications. *Alex. Eng. J.* **2022**, *61*, 10791–10803. [CrossRef]
29. Sayem, A.S.M.; Lalbakhsh, A.; Esselle, K.P.; Moloudian, G.; Buckley, J.L.; Simorangkir, R.B.V.B. Advancements, challenges, and prospects of water-filled antennas. *IEEE Access* **2023**, *11*, 8301–8323. [CrossRef]
30. Yang, X.; Yang, J.H.; Cheng, X.B.; Geng, J.Y.; Qian, B.L. The possibility of using glycerin as the dielectric in pulse forming lines. *IEEE Trans. Dielectr. Electr. Insul.* **2019**, *26*, 339–345. [CrossRef]
31. Gümüş, E.; Yağımlı, M.; Arca, E. Investigation of the Dielectric Properties of Graphite and Carbon Black-Filled Composites as Electromagnetic Interference Shielding Coatings. *Appl. Sci.* **2023**, *13*, 8893. [CrossRef]
32. Omar, M.F.M.; Zubir, I.A.; Kamal, S.; Rajendran, J.A.L.; Mohamed, J.J.; Ahmad, Z.A.; Ain, M.F.; Rahim, S.K.A. A critical review on the development of multi-geometrical stacked wideband dielectric resonator antenna. *Alex. Eng. J.* **2024**, *100*, 111–141. [CrossRef]
33. Mukherjee, B.; Patel, P.; Mukherjee, J. A Novel Cup-Shaped Inverted Hemispherical Dielectric Resonator Antenna for Wideband Applications. *IEEE Antennas Wirel. Propag. Lett.* **2013**, *12*, 1240–1243. [CrossRef]
34. Singh, M.; Ghosh, B.; Sarabandi, K. Analysis of Hemispherical Dielectric Resonator Antenna With an Imperfect Concentric Conductor. *IEEE Trans. Antennas Propag.* **2022**, *70*, 3173–3182. [CrossRef]
35. Petosa, A.; Thirakoune, S. Rectangular Dielectric Resonator Antennas With Enhanced Gain. *IEEE Trans. Antennas Propag.* **2011**, *59*, 1385–1389. [CrossRef]
36. Lu, K.; Leung, K.W.; Pan, Y.M. Theory and Experiment of the Hollow Rectangular Dielectric Resonator Antenna. *IEEE Antennas Wirel. Propag. Lett.* **2011**, *10*, 631–634. [CrossRef]
37. Kishk, A.; Yin, Y.; Glisson, A. Conical dielectric resonator antennas for wide-band applications. *IEEE Trans. Antennas Propag.* **2002**, *50*, 469–474. [CrossRef]

38. Almpanis, G.; Fumeaux, C.; Vahldieck, R. The Trapezoidal Dielectric Resonator Antenna. *IEEE Trans. Antennas Propag.* **2008**, *56*, 2810–2816. [CrossRef]
39. Systèmes, D. *CST Studio Suite 2023*; Dassault Systèmes: Vélizy-Villacoublay, France, 2023.
40. Xing, L.; Xu, Q.; Zhu, J.; Zhao, Y.; Alja'afreh, S.; Song, C.; Huang, Y. A High-Efficiency Wideband Frequency-Reconfigurable Water Antenna With a Liquid Control System: Usage for VHF and UHF Applications. *IEEE Antennas Propag. Mag.* **2021**, *63*, 61–70. [CrossRef]
41. Zhu, R.; Wang, J. A Shape-Changeable Antenna Constructed by Distilled Water for Low-Profile and Low-Radar-Cross-Section Applications. *IEEE Antennas Wirel. Propag. Lett.* **2023**, *22*, 2945–2949. [CrossRef]
42. Jacobsen, R.E.; Lavrinenko, A.V.; Arslanagić, S. Electrically Small Water-Based Hemispherical Dielectric Resonator Antenna. *Appl. Sci.* **2019**, *9*, 4848. [CrossRef]
43. O'Keefe, S.G.; Kingsley, S.P. Tunability of Liquid Dielectric Resonator Antennas. *IEEE Antennas Wirel. Propag. Lett.* **2007**, *6*, 533–536. [CrossRef]
44. Zainud-Deen, S.H.; El-Shalaby, N.A.; Awadalla, K.H. Hemispherical DRA Antennas Mounted on or Embedded in Circular Cylindrical Surface for Producing Omnidirectional Radiation Pattern. *Int. J. Commun. Netw. Syst. Sci.* **2011**, *4*, 601–608. [CrossRef]
45. Ray, S.; Banerjee, A.; Gangopadhyaya, M.; Gupta, B. A Survey On The Effects Of Different Parameters Of Liquid Monopole Antennas Using Different Liquids. In Proceedings of the IEEE Indian Conference on Antennas and Propagation, Jaipur, India, 13–16 December 2021; pp. 766–769. [CrossRef]
46. Roopa, S.; Kumar, E.K. Analysis of conical liquid antenna for wide range of frequencies. *Int. J. Ultra Wideband Commun. Syst.* **2021**, *4*, 197–204. [CrossRef]
47. Abou Shahine, M.Y.; Al-Husseini, M.; Mervat, M.; El-Hajj, A. Dielectric resonator antennas with band rejection and frequency reconfigurability. *Prog. Electromagn. Res. C* **2014**, *46*, 101–108. [CrossRef]
48. Jana, S.; Mandal, S. Design and Analysis of Liquid Based Dielectric Resonator Antenna for Wireless Application. *Int. J. Microw. Wirel. Technol.* **2020**, *12*, 389–395.
49. Low, J.H.; Chee, P.S.; Lim, E.H.; Lee, K.Y. Compact organic liquid dielectric resonator antenna for air pressure sensing using soft material. *Sci. Rep.* **2020**, *10*, 14907. [CrossRef]
50. Varshney, G.; Verma, A.; Pandey, V.; Yaduvanshi, R.; Bala, R. A proximity coupled wideband graphene antenna with the generation of higher order TM modes for THz applications. *Opt. Mater.* **2018**, *85*, 456–463. [CrossRef]

Disclaimer/Publisher's Note: The statements, opinions and data contained in all publications are solely those of the individual author(s) and contributor(s) and not of MDPI and/or the editor(s). MDPI and/or the editor(s) disclaim responsibility for any injury to people or property resulting from any ideas, methods, instructions or products referred to in the content.